Optical Engineering

OpticalEngineering.SPIEDigitalLibrary.org

Review of photomixing continuous-wave terahertz systems and current application trends in terahertz domain

Reza Safian
Galia Ghazi
Nafiseh Mohammadian

SPIE.

Reza Safian, Galia Ghazi, Nafiseh Mohammadian, "Review of photomixing continuous-wave terahertz systems and current application trends in terahertz domain," *Opt. Eng.* **58**(11), 110901 (2019), doi: 10.1117/1.OE.58.11.110901.

Optical Engineering 58(11), 110901 (November 2019)

REVIEW

Review of photomixing continuous-wave terahertz systems and current application trends in terahertz domain

Reza Safian,[a] Galia Ghazi,[a,*] and Nafiseh Mohammadian[b]
[a]imec USA, Kissimmee, Florida, United States
[b]University of Central Florida, CREOL, Orlando, Florida, United States

Abstract. Within the last two decades, terahertz systems have become a well-established tool in scientific laboratories and industrial research and development departments. Unlike the methods of pulsed terahertz radiation that mainly rely on ultrafast optical technology, the technology behind continuous-wave terahertz sources and detectors has a long history involving many different types of technical schemes. The intent is to provide a brief review of the continuous-wave terahertz systems that are based on photomixing and current application trends in the field of terahertz technology. [DOI: 10.1117/1.OE.58.11.110901]

Keywords: continuous-wave terahertz systems; terahertz imaging; terahertz spectroscopy.

Paper 190449V received Apr. 6, 2019; accepted for publication Aug. 26, 2019; published online Nov. 6, 2019.

1 Introduction

Terahertz (THz) frequency band is a region in the electromagnetic spectrum covering frequencies between 0.1 and 10 THz that lies between the microwave and the optical frequency bands. In the literature, it is known as submillimeter radiation, THz waves, T-rays, and T-waves. In the late eighties, development of ultrashort pulse laser technology along with the appearance of THz emitters and detectors made it possible to explore the unique spectroscopy and imaging characteristics of THz frequency band. THz frequency range can provide complementary information to that obtained with microwaves, infrared, visible, ultraviolet, or x-ray that are located on both sides of the THz domain. Compared with radio frequency and microwave which are lower frequencies, THz has the advantage of superior spatial resolution due to the shorter wavelength. On the other hand, the THz frequencies (especially above 1 THz) are too high to be measured using electronic devices. Therefore, they are usually measured using the properties of wavelength and energy. Similarly, the coherent wave generation in this frequency range ceased to be possible by the conventional electronic devices used to generate radio waves and microwaves, requiring the development of new devices and techniques. Not a long time ago, THz frequency band was known as the "THz gap" due to the scarce existence of sources in this frequency band. With the recent advances in this field, different THz sources are available today. Currently, the main sources for THz radiation are electronic sources, photoconductive antennas (PCA), gas lasers, free electron sources and synchrotrons, quantum cascade laser (QCL) sources, nonlinear crystals, and optical rectification in gases.[1]

- Electronic sources such as Gunn diodes, Impatt diodes, and resonant tunneling diodes are able to emit at frequencies up to several THz.[2,3] However, they usually generate sub-THz frequencies and for electronic THz sources, the performance degrades at higher frequencies. Other approach in electronic sources is harmonic generation in nonlinear electronic devices.[4]
- PCAs are suitable both for generation and detection of high-frequency electromagnetic signals.[5] A semiconductor material with a short charge carrier lifetime acts as the source for the antenna. A DC bias voltage is applied to the metallic antenna and a laser beam focused on the region between the metallic stripes generates the free carriers. The semiconductor gap serves as a photoconductive switch in which fast potential change accelerates the free carriers and induces electric current in the antenna, which leads to THz radiation. The antenna length determines the preferred frequency at the resonance condition. For higher output powers, devices with larger areas have been constructed with interdigitated electrodes. Usually in THz systems, a hyperhemispheric or elliptic silicon substrate lens is used for beam shaping.[6]
- Gas lasers also known as optically pumped THz lasers[7] are one of the most powerful sources of continuous-wave (CW) THz radiation. In these lasers, transitions of certain molecules between rotational states generate discrete frequencies in THz range. They typically have output powers of a few mWs and a very low conversion efficiency. The output power is difficult to improve due to the lack of high power tunable midinfrared pumping sources.
- Free electron lasers and synchrotron light sources in which the lasing medium is actually very high speed electrons moving freely through a periodic magnetic structure. They are able to emit very high powers and are tunable in a wide frequency range that includes THz frequencies as well, but they are very large and expensive. Therefore, they have limited use in fundamental physics experiments.[8]

*Address all correspondence to Galia Ghazi, E-mail: Galia.Ghazi@imec-int.com

- Backward-wave oscillator (BWO) tubes are based on the interaction of electron beam with a slow wave structure. An electron gun emits an electron beam that is focused by an external magnetic field. The focused beam interacts with a slow-wave structure that generates a traveling wave that moves backward against the beam. The wave is coupled to the output waveguide near the electron gun. By changing the acceleration voltage, the operating frequency of the device can be electronically tuned from sub-THz to 1 THz frequency range. BWOs offer high output power, good wavefront quality, wavelength tunability, and a high signal-to-noise ratio (SNR), so they have been used as THz sources for imaging systems.[9]
- Nonlinear sources that are mainly based on differential frequency mixing between wavelength components in the broad spectrum of an ultrafast laser.[10] In the case, only a single input beam is used, the method is called optical rectification. In general in these sources, the intensity of THz radiation is proportional to the square of the laser intensity because the differential frequency mixing is a second-order nonlinear optical effects.
- Optical rectification using femtosecond optical pulses in gases (e.g., air) can generate THz wave emission. A plasma is generated by the superposition of an infrared beam with its second harmonic.[11] In comparison with optical rectification in crystals, the emission bandwidth is typically higher, and higher pulse energies can be obtained.
- QCLs are semiconductor lasers that have been originally developed for emitting in the mid- and far-infrared spectral region. Optimization for particularly long emission wavelength has lead to emission frequencies of a few THz. They can emit relatively high-power CW and pulsed waves with the output power reaching up to hundreds of mWs. Such lasers are very compact, but mostly they work at low temperature and need a cryogenic cooling system.[12]

Figure 1 shows power performance of the conventional coherent tunable sources.

Main THz detectors are thermal detectors, electro-optical detectors, and PCAs.

- The earliest THz detectors were bolometers that are thermal sensors that absorb electromagnetic radiation in an active area resulting in an increase of their temperature. They are incoherent sensors which mean that they are not phase sensitive and only provide signal amplitude detection. Because thermal conversion is generally wavelength independent, the measured signals do not depend upon the spectral content of the radiant power. Hence, bolometers can be very broadband detectors. More sophisticated thermal detectors are developed, such as microelectromechanical systems with a metamaterial absorber and a bimaterial (differential thermal expansion).[14,15] These sensors are optimized for specific frequencies at present. All thermomechanical systems are inherently slow.
- Electro-optic sampling detectors[16] in which a THz wave and an optical field interact with each other inside a nonlinear crystal material. This detection method is frequently used in time-domain spectroscopy.
- PCAs can also be used for THz signal detection. Essentially, a kind of pump-probe measurements is performed. An optical probe pulse acts on a photoconductive switch while the THz wave to be detected passes it. The voltage between the two electrodes of the switch will thereafter be proportional to the electric field of the THz wave at the time of the arrival of the probe pulse.

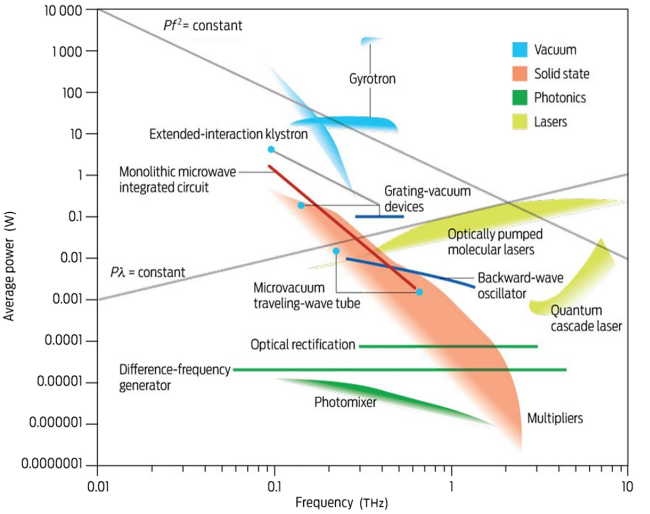

Fig. 1 Power performance of conventional coherent tunable sources.[13]

Figure 2 shows DSB noise temperature performance of superconductor–insulator–superconductor (SIS), hot-electron bolometer (HEB), and Schottky barrier diode (SBD) detectors.

THz systems can be divided into two categories: pulsed wave and CW. Pulsed systems generate a broadband signal that is suitable for THz spectroscopy. THz time-domain spectrometry systems were developed during the late eighties after the invention of the Auston switch, which is a semiconductor device capable of generating and detecting THz radiation,[5] and the availability of near-infrared (NIR) ultrashort

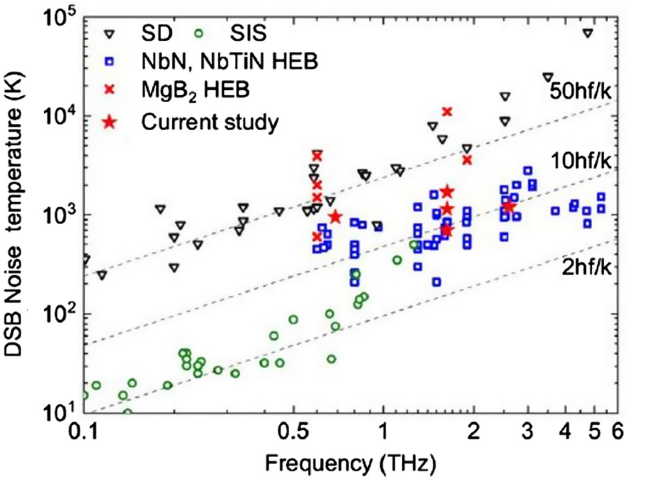

Fig. 2 DSB noise temperature performance of SIS, HEB, and SBD mixers. (SIS, superconductor–insulator–superconductor; HEB, hot-electron bolometer; SBD, Schottky barrier diode).[17]

pulse laser sources. The detected broadband pulse can be analyzed using fast Fourier transform to obtain the spectrum of the signal. On the other hand, THz CW sources produce a narrow band signal that is usually generated by using photomixing techniques or cryogenically cooled QCLs.[18]

Each of the frequency-domain and time-domain techniques has unique advantages and disadvantages. Time-domain systems are relatively more complex and expensive, but they are able to provide useful information that is not accessible in a CW system. In the case, this extra information is imprecise or too difficult to interpret, and the advantages offered by a time-domain system quickly disappear. There are applications where the information provided by a CW system is simply inadequate, in which case one has no choice but to use a time-domain system. Another key advantage of a pulsed THz system is flexibility. All of this information is recorded with one measurement from one detector and can be reprocessed to precisely find the information required for each application. The difference between the two systems is in simplicity and adaptability. For many applications, the additional information is unnecessary, and a pulsed system has no advantage. In performing THz imaging, for CW system, the intensity data are simply stored in a matrix, which can be directly converted to a raster image. The data from the pulsed THz system are more complex and therefore require more advanced processing to be fully utilized.[19] In pulsed THz imaging method, depth information is encoded in the waveform mainly in changes in pulse timing. A change in the temporal location of the reflected peak indicates a change in the optical path length to the substrate. Smaller pulses that are offset from the main peak indicate the existence of scattering centers or interfaces within the sample that are partially reflecting the pulse. The time delay between these secondary pulses and the main pulse can easily be converted to depth.[20,21] CW radiation is also scattered and reflected by these features, and it is possible through the use of additional detectors or by performing additional scans of the sample to recover similar information. By changing the angle of the detector relative to the beam, it is possible to measure scattered light instead of the specular reflection from the substrate. Different angles correspond to scattering and reflection at different locations within the substrate, and thus the scattered intensity can display the features of defects within each measured stratum of the sample.

The challenge for CW systems is to achieve sufficient THz power for applications. PCAs work well in pulsed systems with high peak power at a moderate repetition rate. However, they have limitations as photomixer emitters in CW operation. Using LT-GaAs photomixers, THz power of a few microwatts is reported. The advantages of photomixer devices are the broad tunability, which typically ranges from 0.1 to 3 THz, and the integration that is possible with diode and fiber technologies. The frequency resolution available with photomixers (<1 GHz) is also generally higher than pulsed methods that means that photomixers are often favored for gas spectroscopy. On the other hand, exploitation of telecom technologies for CW THz systems offers alternative devices for THz generation such as photodiodes with integrated antennas. The state-of-the-art performance of conventional coherent tunable THz sources is shown in Fig. 3. Photomixing (or optical heterodyne down conversion) is the one with widest frequency band. With great advances

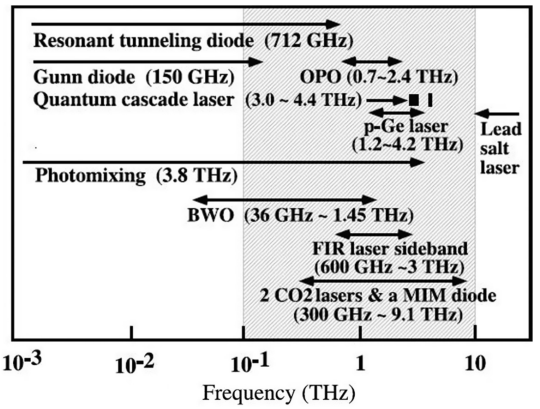

Fig. 3 State-of-the-art performance of conventional coherent tunable sources.[22] (Copyright 2005, Springer.)

in high-speed III-V optoelectronic devices and solid-state lasers, power generation by photomixing has been improved drastically in recent years. Many efforts of optimizing the antenna design and the substrate material of the photomixer have been successful in the improvement of the THz output power. However, there is still much room for output-power improvement. Since photomixing is based on the photoexcitation of the substrate semiconductor, the incident photon energy must be higher than the bandgap energy. Photomixing has been made using the device fabricated on the low-temperature-grown GaAs (LT-GaAs) substrate and using the laser source of which the emitting wavelength is around 800 nm. The technology of diode lasers and optical fiber components which are components necessary for photomixing has progressed remarkably in the optical communication band. The bandgap energy of such materials as Ge and GaSb is lower than the photon energy of the communication band. This situation requires the development of ultrafast photoconductors having such excellent qualities as the LT-GaAs in the communication band.

In the following sections, after a brief review of the applications of the CW THz systems, different system topologies that are currently used in CW THz systems are reviewed.

2 Applications of Terahertz Waves and Emerging Technologies

THz technology is applicable to various domains that provide unprecedented capabilities for many research fields. Some of these application domains are biology, pharmaceutics, security-related areas,[23,24] paper production processes,[25] tissue burn reflectometry,[26] detection of tooth cavities,[27,28] industrial nondestructive evaluation, material science and spectrometry,[29–34] environmental monitoring, security, and astronomy, semiconductor device diagnostics,[35] trace gas analysis, moisture analysis for agriculture,[36,37] quality control of packaged goods, cultural heritage inspection,[38,39] and many other disciplines of physics and chemistry. Information and communication technologies have also a strong potential to benefit from THz technology in wireless communication, high speed data processing, and satellite communications. THz imaging and spectroscopy have been applied to huge variety of materials in numerous fields in order to determine the potential of this emerging technology and subsequent development of systems. Researchers are still working on new ways to exploit the unique properties of THz

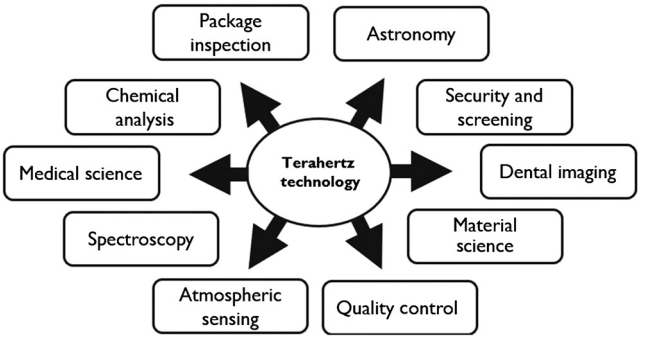

Fig. 4 Explored and future THz technology applications.

frequencies in real life applications. Figure 4 shows some of the current and future applications of THz technology.

THz radiation interacts strongly with polar molecules, such as water, which absorb THz radiation. This limits penetration of the radiation in moist substances, on the other hand, making it readily detectable even in very low concentrations. For this reason, THz waves can provide a better contrast for soft tissues than x-rays. THz radiation can penetrate most dielectric materials and nonpolar substances such as wood, paper, cloth, and plastic. THz radiation is totally reflected from metallic surfaces and partially reflected from interfaces between nonmetallic materials with different refractive indices, enabling objects to be detected beneath various surfaces. The interesting fact about THz frequencies is that many molecules present strong absorption at THz frequencies and therefore can be identified by spectroscopy. In the following part of this section, a brief review of some of the THz technology applications and some of the commercial companies that are active in this domain are reviewed.

2.1 *Process Analytical Technology and Nondestructive Testing*

Process analytical technology (PAT) is a system for designing, analyzing, and managing the manufacturing process. The United States Food and Drug Administration (FDA) has published guidelines for introducing PAT into pharmaceutical production. Consequently, there is an increasing need for the analysis of medicines to reassure consumers and increase safety. Also the polymer processing industry is continuously investigating new process control and nondestructive testing techniques.[40–43] Many plastic materials are transparent to THz radiation and serve as a base material for passive THz system components. In return, THz systems can reveal valuable information of the composition of polymers. Offline measurements for the characterization of molecular properties, considering the following inline process monitoring with real-time feedback, and referring finally to quality inspection of the polymeric components are some of the applications of the THz technology in polymer industry.[44]

2.2 *Passive Spectroscopy and Astronomy*

CW THz systems have also been used in the field of astronomy for the past few decades for passive spectroscopy. THz waves can penetrate in a solid and can be used to discriminate intermolecular interactions between molecules or crystals inside the solid. For THz frequencies above 1 THz, there are many vibration modes of molecules or crystals that occur due to intermolecular interactions. Consequently, the spectral fingerprint, in which the vibration modes absorb THz waves, allows us to identify the materials. The molecular interaction is stronger as the frequency increases; however, the penetration of THz waves within solids tends to decrease because the shorter wavelengths at higher frequencies are easily scattered by particles. Therefore, there is a limited region inside the frequency range from 0.3 to 5 THz where the two advantages of deep penetration and spectral fingerprint are both obtained. Even within the THz spectrum in the low frequency region of 0.1 to 0.3 THz, it is difficult to identify molecules or crystals even though penetration is easy, whereas in the higher frequency region of 5 to 10 THz, extremely high loss limits the available sample thickness within thin films or surfaces.[45]

2.3 *Reflection and Stand-Off Imaging*

CW THz imaging is advantageous for specific applications due to its higher single-frequency dynamic range and the nature of possessing a narrow spectral bandwidth. One important advantage of imaging with a single-frequency source is the ability to select the source wavelength to optimize the imaging capability. This is very useful in the case of imaging at a stand-off distance since at greater than a few meters distance. Stand-off imaging is challenging because of the presence of atmospheric water vapor, which significantly attenuates the THz beam. However, at certain frequencies within the THz range, the atmospheric attenuation is minimized because there are no nearby strong water vapor absorption lines. The ability to tune the THz source to a water window is a considerable advantage. For example, for a 25-m stand-off, the power throughput from transmitter to receiver increases by more than a factor of 10 if the atmospheric loss decreases by 0.5 $dB.m^{-1}$.[46] Real-time imaging at a 25-m stand-off has been demonstrated using a THz QCL and a room-temperature microbolometer array.[6,9,11,16,19,20,23,25,26,35,36,39,40,46–82] In addition, because time-delay scan is not a compulsion requirement in a CW system, the acquisition speed of a CW THz imaging system can be increased relative to that of a pulsed system, in which time-delay scanning is generally necessary.

CW imaging is first demonstrated by Siebert et al.[83] and Kleine-Ostmann et al.[84] Siebert et al. employed the room temperature optoelectronic detection scheme of photomixing two CW lasers in a photoconductor. They used a 200-ms lock-in time constant and measured a signal-to-noise ratios of 100:1. However, femtosecond lasers are typically complex and expensive. In Ref. 84, an imaging system using a two-color external-cavity laser diode is presented. They measured images of biological tissue, with an SNR of around 75:1. Detection was achieved using a bolometer which is typically not phase sensitive and severely limits the modulation bandwidth. From a commercial perspective, using a Ti:Sapphire laser and bolometric detection respectively which needs expensive laser sources and cannot perform room-temperature phase-sensitive detection. Gregory et al.[71] demonstrated a compact CW THz imaging system that combined diode lasers with optoelectronic detection.

Currently, there are two methods that are commonly used for CW THz imaging: a raster scan of a focused incident beam, or the formation of an image on a detector array. In the former, a single detector, such as a Schottky diode,

Golay cell, or pyroelectric detector, is used to detect the full power of the beam. This has the advantage of a high dynamic range, but the disadvantage is that the image must be formed point by point using a scanning system, which is time-consuming and not applicable to moving targets. The development of a sensitive THz detector array is still an active research area. Detector arrays also have the disadvantage of being severely affected by distortions and aberrations in the focusing system, whereas for a raster scanning system, the beam can be focused to a diffraction-limited spot. In general, a CW system can outperform systems based on time-domain photoconductive sampling in frequency resolution, spectral brightness, system size, and cost.

2.4 *Medical Imaging*

It has been shown in recent years that THz transmission imaging can be used to generate three-dimensional (3-D) visualization of objects' internal structure, which can be valuable for biological imaging applications. Other use case for 3-D THz imaging could be the noninvasive analysis of archeological findings, such as inspection of paintings, wrapped mummies,[85] or human bones.[51] Many techniques have been investigated for the acquisition of 3-D images at THz frequencies, including diffraction tomography,[62] use of binary lenses,[86] time-of-flight measurements in reflection mode and tomosynthesis,[87] and more recently computed tomography (CT) with ultrashort THz pulses,[52] or CW sources.[54] THz tomography competes against the longtime used Xray CT, which usually provides high spatial resolution and high contrast images. However, there are three opportunities for THz frequencies in this field. First, THz waves may provide valuable supplemental information, enabling additional extraction of the spectroscopic object properties[52] and providing different absorptive contrast as compared to x-rays. Second, ongoing advances in silicon-integrated THz components and photonic circuits should enable the realization of ultra-low-cost 3-D THz-CT imaging systems,[76] which promises an increased exploitation for future industrial applications as compared to expensive x-ray machines. Third, THz waves do not ionize the samples as they go through them which makes them less risky and more suitable for biological detections and medical imaging.[49,88] More importantly, a better image contrast for biological soft tissues can be obtained by the THz imaging technique[80,89] thereby getting more accurate and comprehensive structural views and biological information. In a recent paper, the authors demonstrated the use of a CW THz CT system to reconstruct two-dimensional (2-D) cross-sectional images of the chicken ulna to visualize the internal structure of it.[90] Compared with the pulsed THz CT systems,[62,91] the CW THz system is more compact and low cost. The proposed CW THz CT system is shown in Fig. 5 which is based on BWO that can produce a CW THz and a Golay cell detector. The testing chicken ulna is fixed on the precision electric rotation stage and the electric 2-D translation stage, and it is rotated and translated during the recording process of projection data and they have looked at the effect of different projection angle intervals on the quality of the images. In Fig. 6, the optical photographs of sections II and IV of the chicken ulna using the optical microscope and THz imaging are shown. Since the internal substance of the chicken ulna has different absorptions for the THz wave, the internal structure distribution and

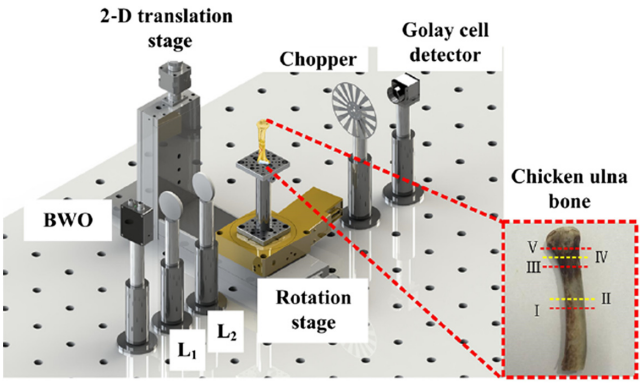

Fig. 5 The setup of CW THz CT with BWO and Golay cell detector.[90]

profile information of the chicken ulna can be obtained in the 2-D cross sectional images by the CW THz CT system.

Protein and DNA molecules typically have intramolecular vibrations in the THz range. High hydration level to ensure homogeneous samples results in a large water background that increases the protein THz absorbency. Lack of narrow resonances for unoriented samples prevents use of THz for protein or DNA identification. Using linear dichroism measurements on protein crystals, distinct narrow resonances unique to both the protein and protein binding state have been observed.[81] The ability to measure the intramolecular vibrations is a necessary tool to resolve the ongoing argument of their role in biological function. Also, interpretation of the resonant bands will be a challenge, as these consist not of single vibrations, but sets of vibrations with the same polarization dependence.[60]

Rapid and accurate detection is essential for early diagnosis and cell activity monitor. Current cell detection methods mainly depend on labeling technology, such as flow cytometry, fluorescence molecular tomography, and multiphoton microscopy, with high sensitivity, precision, and selectivity. However, biological labeling can directly affect the biological activity and function of living cells. This fundamentally limits the ability of existing cell detection to molecular level resolution. Although the label-free cell detection method including electrochemical and piezoelectric technologies has been applied widely, potential radiation hazard and limited sensitivity still make them controversial. Hence, an alternative method for a label-free and noninvasive cell viability evolution is urgently needed for life sciences.[50] THz spectroscopy is developing into an optical, noninvasive, label-free, and reagent-free technique, which can be utilized for detection and identification of living cells.

One of the growing applications of THz technology is bacterial detection. Based on small size and low absorption coefficient of the bacteria, THz radiation can propagate through an entire object, allowing bacterial components contribute to the THz signature of objects. Extensive researches were conducted to realize qualitative and quantitative analyses of bacteria. The sensitive detection of bacteria in both ambient and aqueous environments is feasible using THz metamaterials (Figs. 7 and 8). A THz metamaterial based on the SRR pattern of 550-mm high resistance silicon substrate was used for high-sensitivity detection of bacteria in solid and liquid phases.[50]

Several THz imaging systems have been developed for the noninvasive detection of tissues to assess the depth and

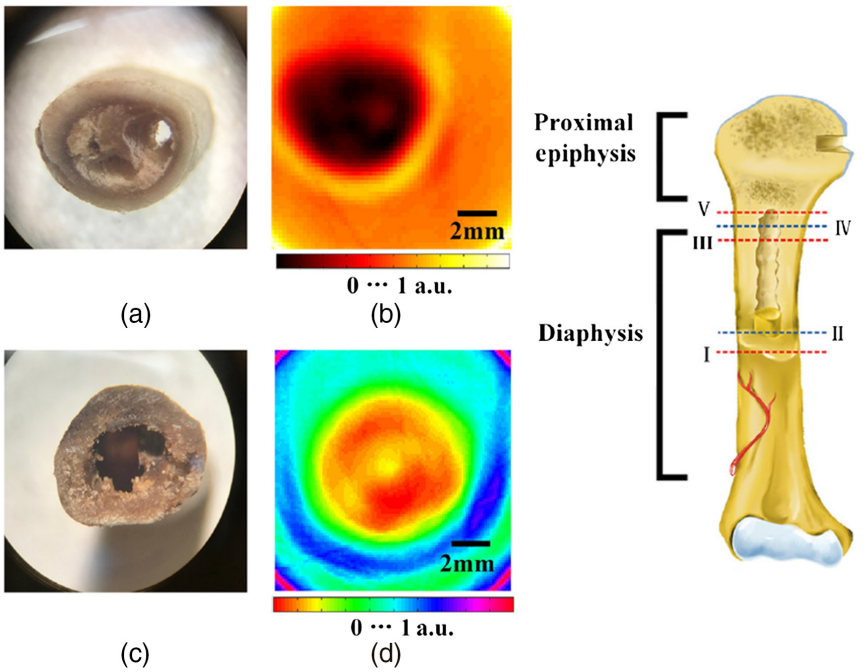

Fig. 6 The optical photographs and 2-D cross-sectional images of the chicken ulna at sections (a) and (b) II and (c) and (d) IV in the schematic diagram of the chicken ulna.[90]

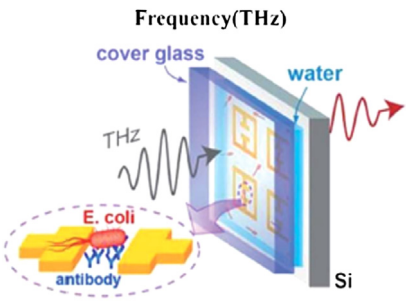

Fig. 7 A schematic of specifically selective bacteria detection using metamaterial in solution environment.[50]

severity of burned tissues. Because the cancerous or other diseased tissues can contain higher water content as a result of increased vascularity or edema, THz imaging has shown potential in differentiating tissue types. A recent simulation study found that InN-enhanced THz imaging enables highly sensitive diagnosis of early-stage skin cancer based on tiny water content changes.[50,92] The water contents of blood vessel and corneal tissue were also resolved using a THz imaging system.[93] Furthermore, the difference among various tissues is still significant after formalin fixing, suggesting that the difference is due to changes in water content and structural changes. Moreover, based on higher THz reflection intensities, fresh human early gastric cancer tissues have been distinguished from normal mucosa, (Fig. 9).[94] Interestingly, it is successful that the imaging of human

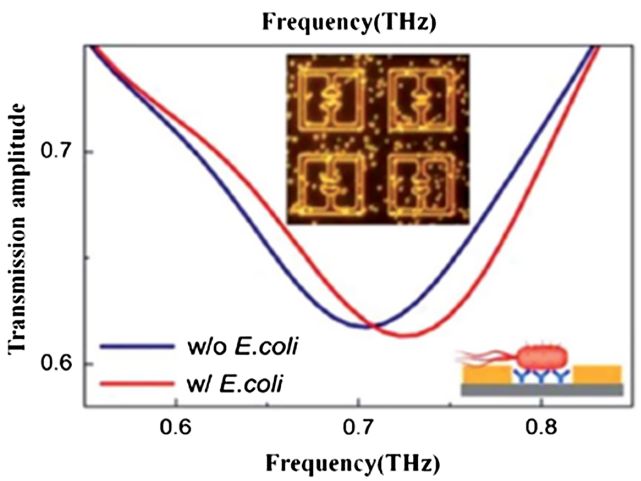

Fig. 8 THz transmission with and without the deposition of *E. coli* using the functional metamaterials in aqueous environments.[50]

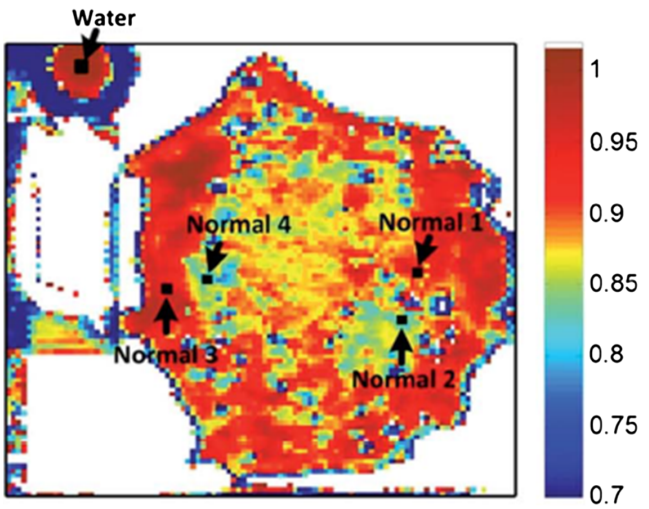

Fig. 9 THz image of tissues from early gastric cancer.[50]

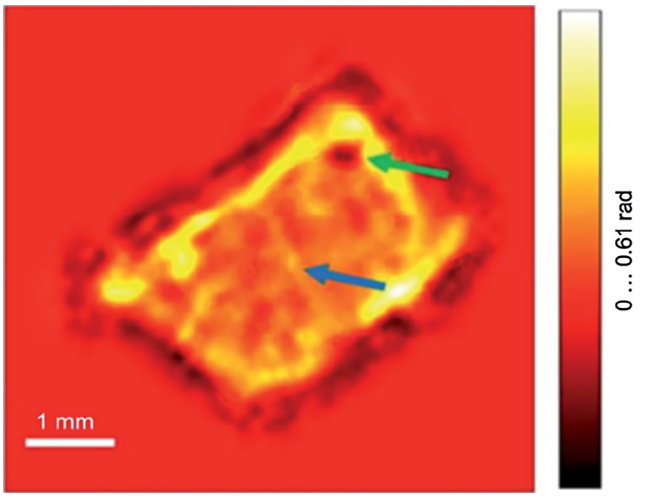

Fig. 10 THz in-line hologram of human hepatocellular carcinoma tissue by phase-shift distribution reconstructing.[50]

hepatocellular carcinoma tissue has been obtained using CW THz digital in-line holography in the absorption and phase-shift distributions (Fig. 10).[80] By rejecting Fresnel reflections, the cross-polarized THz image of nonmelanoma skin cancer displays the approximate location of the tumor clearly.[79]

2.5 *Pharmaceutical Applications*

Some of the recent pharmaceutical applications of THz are (1) discrimination and quantification of hydrates, (2) analysis of solid form transformation dynamics, (3) quantitative characterization of tablet coatings: off-line and on-line, (4) tablet coating and dissolution, and (5) spectroscopic imaging and chemical mapping. TeraView has applied its proprietary THz imaging and spectroscopy technology to increase pharmaceutical product and process understanding as an effective part of the quality by design initiative. Their 3-D THz imaging system is able to nondestructively estimate critical quality attributes in pharmaceutical products, such as crystalline structure, thickness, and chemical composition. Their THz imaging system monitors the impact of changing the solids level of a coating suspension from 15% to 25%, which reduces the coating process time. Figure 11 shows some sample results in which a change in adhesion between the substrate and coating.

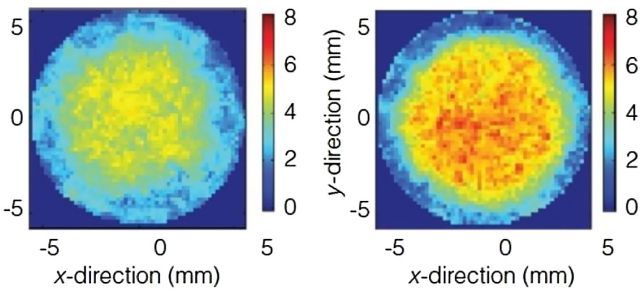

Fig. 11 The 2-D THz image of a tablet to investigate the effects of film-coating process on a finished drug product.[95]

2.6 *Noncontact Imaging for Conservation of Paintings, Manuscripts, and Artifacts*

Recently artwork started to be scanned by THz systems.[57] These imaging systems have been used for scanning ancient mummified samples paintings.[74,75] Frequency-domain THz systems allow for the depth inspection of the object under investigation due to the frequency sweep of the emitted radiation.[74] Figure 12(a) shows the THz image of the global maximum of the signals recorded from the contemporary painting after contrast enhancement.[57] By comparing it with the THz surface topography of the painting obtained by illuminating the object with raking light Fig. 12(a), it can be seen that the black lines of the THz image correspond to the sharp edges of the thickest brushstrokes used by the artist to model the subjects in relief. Figure 12(b) shows the signals recorded at (x, y) coordinates corresponding to low [in correspondence of the sharp edges, green and red curves in Fig. 12(c)], medium [yellow and orange curves in Fig. 12(c)], and high [blue and violet curves in Fig. 12(c)]

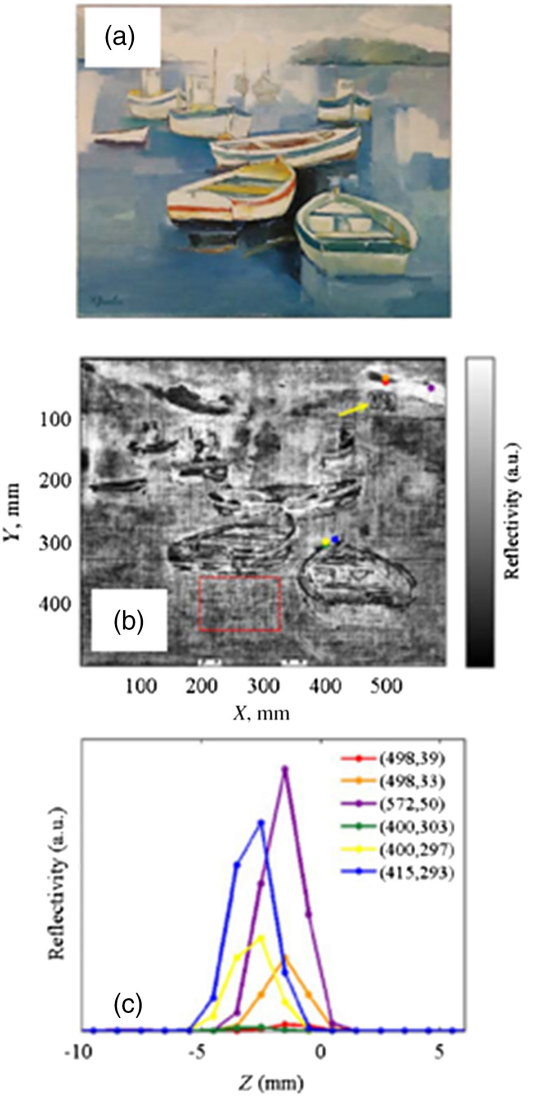

Fig. 12 (a) The contemporary painting front, (b) THz image of the contemporary painting after contrast enhancement, parameter: signal global maximum, (c) signals recorded at the (x, y) coordinates reported in the legend, corresponding to the colored dots of Fig. 12(b).[57]

reflectivity values, which have been collected from neighboring pixels in two different areas of the painting.

2.7 *Terahertz Communication*

Wireless data traffic has been expanding in the past few years. In particular, mobile data traffic is expected to increase sevenfold between 2016 and 2021 due to increase in whereas video traffic. Such remarkable growth of wireless traffic has driven the urge to investigate suitable regions in the radio spectrum to fulfill the accelerating demands. To this end, the THz frequency band has received considerable attention in the research fraternity.[61] As a result of the exponential growth of wireless traffic, the demand for higher bandwidth never seems to subside before the capacity of the generation beyond 5G technology has reached its upper limit. THz communications are expected to enable the seamless interconnection between ultrahigh-speed wired networks, achieving full transparency and rate convergence between wireless and wired links. This will facilitate the use of bandwidth-intensive applications across static and mobile users. Some specific applications are high-definition holographic video conferencing (virtual reality office) or high speed wireless data distribution in data centers. Figure 13 shows a schematic of the application of THz back haul links in future cellular networks.[96]

2.8 *Commercial Terahertz Companies*

The Global Terahertz Market is valued at USD 0.09 billion in 2016 and is expected to reach a value of USD 0.67 billion by the end of 2022 (based on Orbis Research Report[97]). THz technology was initially used in very few areas such as planetary science and astronomy. Recent innovations in this technology enabled its spread across many areas such as food and agriculture, pharmaceutical manufacturing, plastics and ceramics, and communications. Recent developments in THz device technology such as generation of THz pulse for spectroscopy applications user NIR laser, low loss waveguide circuits, submicron-scale lithography, and silicon micromachining, which is used for compact and integrated packing, offer a plethora of opportunities. A recent increase in the number of manufacturing companies, and a rise in worldwide demand for precise security systems, defense, and medical sectors are driving the global THz technologies market. However, the high cost is the main obstacle for market growth. Based on the type of technology, the market is categorized as THz imaging (active and passive systems), THz spectroscopy (time- and frequency domains), and communication systems (modulators, emitters, and antennas). Based on end-user application, the market is segmented into medical and healthcare, nondestructive testing, defense, and agriculture. Currently, North America holds the major market share and Asia-Pacific is expected to grow at a considerably high rate. Major global market players in the THz market are Advantest Corporation, Traycer, Terasense, Microtech Instrument Inc., Menlo Systems GmbH, Gentec Electro-Optics, Teraview, and Toptica Photonics AG. In the following, a brief introduction to each of these companies (in alphabetic order of the company name) is provided.

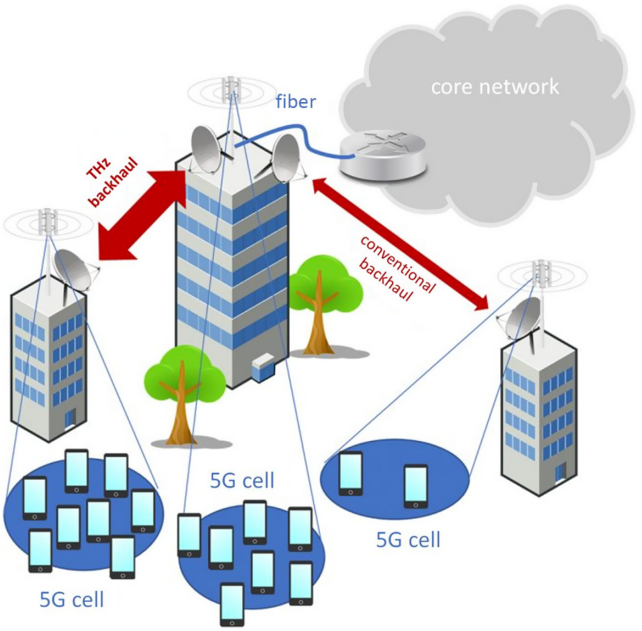

Fig. 13 Application of THz backhaul links in future cellular networks.[96]

Advantest[98] offers a series of low-cost, all-purpose THz spectroscopic systems that enable spectroscopic measurements. The tools are capable of performing nondestructive analysis on a wide variety of sample types, making it applicable to a broad range of fields from life sciences to electronics, where precise chemical and material characterization is critical. The systems are ideal for settings ranging from basic research to product development, as well as for manufacturing and quality control, and employ easy-to-use spectroscopic methods that do not require specialized knowledge of THz-wave generation or optics. One example is the TAS7400 product line (Fig. 14), which is capable of performing nondestructive analysis on a wide variety of sample types, making it applicable to a broad range of fields from life sciences to electronics, where precise chemical and material characterization is critical. The systems are ideal for settings ranging from basic research to product development, as well as for manufacturing and quality control, and employ easy-to-use spectroscopic methods that do not require specialized knowledge of THz wave generation or optics.

Gentec Electro-Optics produces different components for THz power measurement. The company offers pyroelectric-based THz measurement systems that are very easy to use at room temperature. As an example, the T-RAD (Fig. 15) is a microprocessor-based digital radiometer that includes a 12-bit ADC and powered by a USB connection, which also acts as a virtual COM port. The LabView software supplied with the device makes it very easy to set up the radiometer, measure a THz or broadband source and record data.[63]

Menlo Systems GmbH[99] produces high-speed THz scanning systems without out any mechanically moving parts and a large scanning range of nanoseconds. As an example, the compact THz spectrometer TeraSmart (Fig. 16) integrates the latest achievements in broadband THz time-domain spectroscopy into an easy-to use turnkey solution. The modular design based on our OEM laser platform ensures a flexible configuration of the system to meet the needs for integration in any industrial or scientific environment. Custom fiber lengths to THz emitter and detector are available. Moreover,

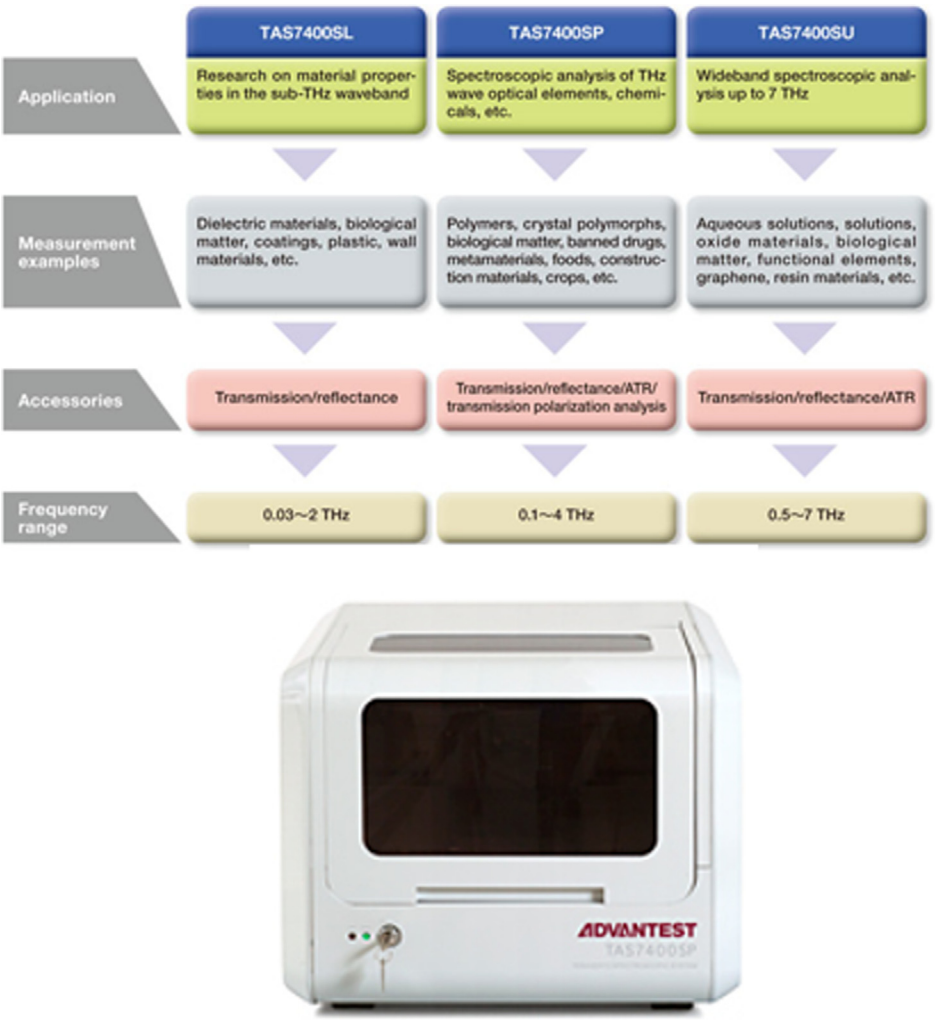

Fig. 14 A full product line-up of TAS7400 product line.[98]

Fig. 15 T-RAD is a microprocessor-based digital radiometer from Gentec.[63]

multibranch configurations are possible, enabling simultaneous measurements of several emitter/detector pairs using only one fs fiber laser oscillator.

Microtech Instrument Inc.[100] produces different THz spectrometers, generators, detectors, and passive components. One of their interesting products is T-Vision system which is video rate imaging system. It is the solution for imaging applications that require high frame rates. The T-Vision system is an all-in-one system based on a nonlinear process, where the THz image is mixed with a near-IR pulse, generating an upconverted near-IR image that is detected with a CMOS camera (Fig. 17).

National Optics Institute (INO)[78] is another company that offers THz illumination source especially designed to build a complete THz imaging system when paired with INO's THz camera. Their THz imaging system can be used for both see-through imaging (transmission imaging) and reflection mode. One example of their products is MICROXCAM-384i-THz THz camera that allows you to see through materials in real time. It is based on INO's 384×288 pixel uncooled microbolometric detector, optimized for the THz waveband (Fig. 18).

Terasense Group Inc. is one of the leading manufacturers of portable THz imaging systems with products. Terasense

Fig. 16 TeraSmart, a compact industry-proven THz spectrometer from MenloSystems.[99]

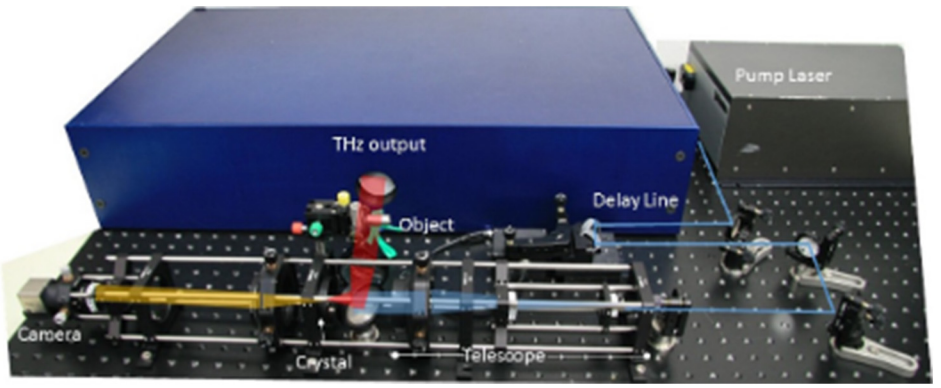

Fig. 17 T-Vision imaging system from Microtech.[100]

Fig. 18 T-Vision imaging system from Ino.[78]

Fig. 19 TeraFAST-256: a THz imaging camera from Terasense.[101]

makes new type of semiconductor detectors for imaging sensor arrays, which effectively cover sub-THz and THz ranges of electromagnetic spectrum (50 to 700 GHz). The company has developed and patented a ground-breaking technology for making new-generation semiconductor imaging systems for THz and sub-THz frequency ranges. As an example, one of imaging cameras produced by this company is TeraFAST-256 system (Fig. 19), which has image acquisition rate of 5000 fps (5 KHz) and scanning speed up to 15 m/s (900 m/ min) with 256 pixels (256 × 1 array of detectors).[101]

Fig. 20 TeraScan: frequency-domain THz platform from Toptica.[102]

TeraView[95] is solely focused upon the application of THz light to provide solutions to customer issues. TeraView has developed its proprietary technology across a number of markets such as fault analysis and quality assurance for semiconductor chips used in mobile computing and communications, nondestructive inspection of high value coatings used in the automotive, pharmaceutical, food and solar industries. As an example, the EOTPR 3000 is one of their products. The system is configured with a manual probe station to meet today's tough FA environment, which requires to isolate fault location in minutes rather than hours or days, while maintaining the EOTPR's world leading sub-5 μm fault isolation accuracy.

Toptica[102] has been working with leading researchers in the THz arena from day one and is now able to serve scientists and engineers working with the two most important optoelectronic approaches—pulsed and CW THz generation. The company manufactures different frequency-domain, time-domain, and THz screening platforms. For frequency-domain THz spectroscopy, Toptica offers two systems—TeraScan 1550 and TeraScan 780 (Fig. 20). Based on precisely tunable distributed feedback (DFB) lasers, digital control electronics, and latest GaAs and InGaAs photomixer technology, the TeraScan systems combine ease of use with best-in-class specifications.

Tracer[103] has been one of the leaders in THz knowledge since 2008, developing unique IP for the detection, imaging, and creation of THz light. One of the company products is (Fig. 21) a real-time (25-100 Hz) imager with a commercial name "THEIA" for THz application development with a large formal focal plane array with integrated readout electronics can be deployed with electronic or photonic sources and application-specific optics. THEIA is designed to integrate into most optical setups for the THz or submillimeter wave researcher or application developer.

3 Continuous-Wave Terahertz Systems Based on Photomixing

Figure 22 shows a typical CW THz measurement setup based on photomixing. In a photomixing system, the optical beat signal generated by a pair of slightly detuned CW lasers is used to modulate the carrier density of the photomixer. This results in a modulated photocurrent,[32] which is coupled out as a CW THz wave by means of an antenna. The main advantage of the photomixing technique is that the output frequency can accurately tuned based on the different frequency of the two pump lasers. On the other hand, the main

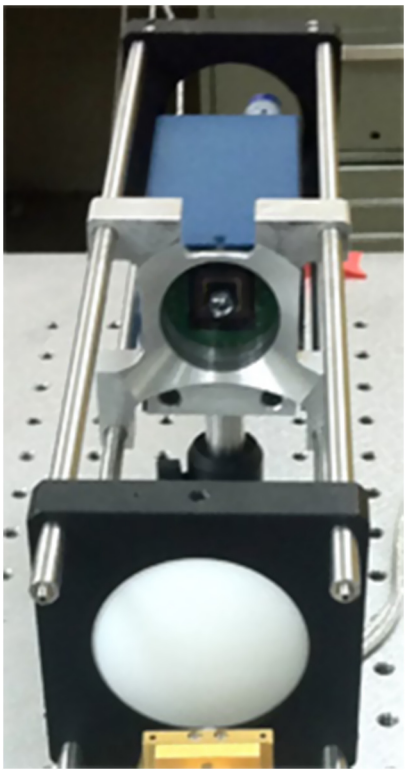

Fig. 21 THEIA: a real-time (25 to 100 Hz) imager Tracer.[103]

disadvantage to overcome in this technique is its low conversion efficiency. Conversion efficiency of the photomixing is inversely proportional to the duty ratio of the pump laser when the same averaged power is used. Therefore, the primary disadvantage of the photomixing method is that the output power is relatively low compared with other techniques of CW THz generation. Its optical-to-THz conversion efficiency is 10^{-6}–10^{-5}, and the typical output power is in the microwatt range. A typical photomixer includes an antenna structure of metal on a silicon substrate. A silicon lens is attached to the back side of the substrate to focus the THz wave.

In a photomixing THz source, the optical field at the excitation point of the antenna is

$$E_{\text{opt}} = E_1 \exp(-j2\pi\nu_1 t) + E_2 \exp(-j2\pi\nu_2 t + \phi), \tag{1}$$

where E_1 and E_2 are the electric field amplitudes of the two lasers and ν_1 and ν_2 are the frequencies of the two CW lasers, respectively. ϕ is the relative phase between the two optical waves. Thus, the optical intensity at the photomixer is given as

$$I_{\text{opt}} = \frac{cn\epsilon_0}{2}|E_{\text{opt}}(t)|^2, \tag{2}$$

where n is the refractive index of the medium, c is the speed of light in vacuum, and ϵ_0 is the vacuum permittivity. Therefore,

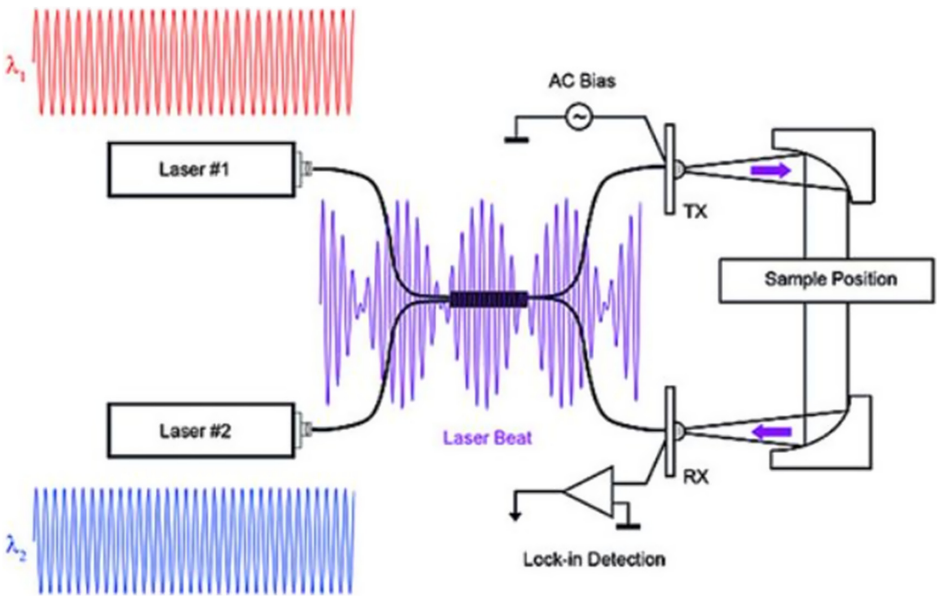

Fig. 22 CW THz measurement setup. λ_1 and λ_2 are the wavelengths of the lasers. Tx is the THz transmitter. Rx is the THz receiver.[104]

$$
\begin{aligned}
I_{\text{opt}} &= \frac{cn\epsilon_0}{2}[E_1^2\cos^2(2\pi\nu_1 t) + E_2^2\cos^2(2\pi\nu_2 t+\phi) \\
&\quad + 2E_1E_2\cos(2\pi\nu_1 t)\cos(2\pi\nu_2 t+\phi)] \\
&= \frac{cn\epsilon_0}{2}[E_1^2/2 + E_2^2/2 + E_1^2/2\cos^2(4\pi\nu_1) \\
&\quad + E_2^2/2\cos^2(4\pi\nu_2+2\phi) \\
&\quad + E_1E_2\cos^2(2\pi(\nu_1+\nu_2)+\phi) \\
&\quad + E_1E_2\cos^2(2\pi(\nu_1-\nu_2)+\phi)]. \qquad (3)
\end{aligned}
$$

There is no material or device that can respond to the instantaneous intensity of first and second harmonics. For the case of a photomixer, the fast oscillating terms from the third to fifth are ignored because of the slow response of the photomixer. Therefore, for the photomixing, it suffices to consider the averaged optical intensity (a DC term) and the optical beat intensity with the difference frequency, $\nu_1-\nu_2$. The optical intensity of these components is

$$
I_{\text{opt}} = I_1 + I_2 + I_B, \quad I_B = 2\sqrt{I_1 I_2}\cos[2\pi(\nu_1-\nu_2)t+\phi], \qquad (4)
$$

where I_1 and I_2 are the intensity of the two lasers and I_B is the intensity of the beat frequency $(\nu_1-\nu_2)$. Hence, THz radiation is obtained when the difference frequency is tuned to the THz frequency range. We also can calculate the optical power incident on the photomixer as[105]

$$
\begin{aligned}
P(t) &= \int cn\epsilon_0 I(t)\mathrm{d}S \\
&= P_1 + P_2 + 2\sqrt{mP_1P_2}\cos[2\pi(\nu_1-\nu_2)+\phi], \qquad (5)
\end{aligned}
$$

$$
P_i(t) = \int cn\epsilon_0\frac{E_i^2}{2}\mathrm{d}S \quad (i=1,2), \qquad (6)
$$

where m is the spatial-mixing efficiency of the two beams, P_i are averaged powers of the two beams. The integration is carried out over the beam cross section. The spatial-mixing efficiency m varies from 0 (no overlap) to 1 (complete overlap).

In a PCA, the beating frequency generates a THz radiation power as[105]

$$
P_{\text{THz}}(\nu) = \frac{1}{2}R_A\frac{1}{1+\omega^2\tau_c^2}I_A^2 = \frac{1}{2}R_A\frac{1}{1+\omega^2\tau_c^2}\tau_c^2\mu_e^2E_{\text{DC}}^2I_B^2, \qquad (7)
$$

where R_A is the radiation resistance, τ_c is the carrier lifetime of the photoconductive material, and μ_e is the mobility of electrons. The radiation power increases quadratically with the optical power I_B and the bias field E_{DC}. I_A is the amplitude of the AC current flowing through the antenna

$$
I_A = \tau_c\mu_e E_{\text{DC}}I_B. \qquad (8)
$$

The radiation resistance corresponds to the real part of the antenna load impedance as

$$
Z_{\text{Re}} = R_A/[1+(\omega R_A C_A)^2]. \qquad (9)
$$

Therefore,

$$
P_{\text{THz}}(\nu) = \frac{1}{2}\frac{1}{1+\omega^2\tau_c^2}\frac{1}{1+\omega^2R_A^2C_A^2}R_AI_A^2. \qquad (10)
$$

Assuming similar photomixer at the detector, the photocurrent I_R in the receiver photomixer is proportional to the amplitude of the incident THz electric field, E_{THz}, and the phase difference $\Delta\phi$ between the THz wave and the optical beat[106,107]

$$
I_R\alpha E_{\text{THz}}\cos(\Delta\phi), \quad \Delta\phi = 2\pi\nu\Delta L/c, \qquad (11)
$$

where ΔL is the difference between the length of the receiver arm and the length of the emitter arm including the THz path.

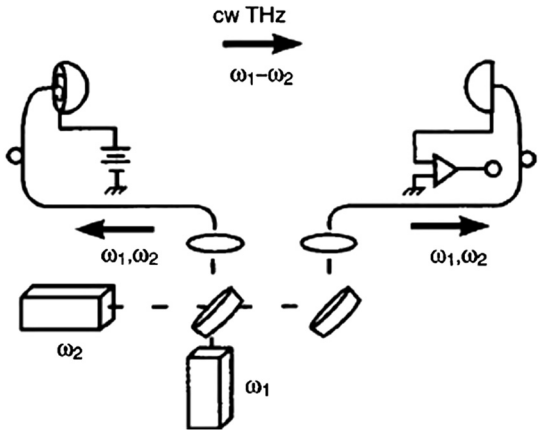

Fig. 23 Schematic of the quasioptical implementation. Two CW Ti: sapphire lasers were used since their tuning range exceeded that of the available diode lasers. A pair of tunable diode lasers was used previously with this setup.[107] (Copyright 1998, American Institute of Physics.)

For the first time in 1998, an MIT research group demonstrated THz coherent detection[107,108] using photomixing. In their transmission mode setup, they used planar log-spiral antennas on LTG-GaAs surface as transmitter and receiver. The size of the active area is 8×8 μm and antenna electrodes were separated by 0.8 to 1.5 μm gaps at transmitter and receiver. Silicon hyperhemisphere lenses are placed on both antennas and the lenses are separated by 6 cm. Two tunable CW Ti:Sapphire lasers are combined with a beam splitter. Input power of each photomixer was ~35 mW and the transmitter was dc biased at 15 V (300 mA current). A schematic of the system is shown in Fig. 23.

As mentioned earlier, at THz frequencies (higher than 1 THz), no detector is able to follow the signal variation in time. Therefore, phase $\Delta\phi$ information cannot be measured directly. Hence, based on Eq. (11), extracting the amplitude information E_{THz} requires a variation of $\Delta\phi$. In the following, a summary of different THz frequency-domain systems that are used to measure the amplitude and phase of the THz signal, which is reflected from a sample (reflection geometry) or transmitted through a sample (transmission geometry) are reviewed.

3.1 *Delay Line Systems*

A simple way to extract the amplitude information of a THz signal is a variation of phase using a delay stage in the THz or optical beam path.[59,65,71,72,83,107–112] Main problem of this simple implementation is that it is slow. Because velocity of a mechanical translation stage is limited to a few millimeters per second. In the delay line setup, the scanning delay in the detector or THz beam path generates an interferogram in the time domain by varying the phase relationship between the incoming THz beam and the beat in the optical field at the receiver. The detected signal varies with the time delay, t', between the THz and optical beams according to the autocorrelation function:

$$E_{\mathrm{THz}} \propto \int_{-\infty}^{+\infty} \cos(2\pi\nu t)\cos[2\pi\nu(t+t')+\phi]\mathrm{d}t. \tag{12}$$

Averaged over THz time scales, the delay line system generates a sinusoidal variation at the THz frequency, and both amplitude and phase can be recovered at each pixel.

The detected THz signal power is very low (usually in μW range). Signal averaging and lock-in detection are the two techniques that are used to achieve a acceptable SNR. In the signal averaging method, each measurement is done several times and then averaged. This almost eliminates the random noise of the detected signal and increases the SNR. But the measurement time is increased drastically. In the lock-in detection method, either a mechanical chopper included into the optical or the THz path or the DC bias of THz emitter has to be modulated. Assuming the chopper or the bias voltage is modulated at frequency ω [$V_{\mathrm{sig}} = \cos(\omega t)$], based on the THz path parameters, the detected signal will have an additional phase ϕ [$V_{\mathrm{det}} = V_s \cos(\omega t + \phi)$]. Multiplying the reference signal with the detected signal

$$\begin{aligned} V_{\mathrm{sig}}V_{\mathrm{det}} &= V_s \cos(\omega t)\cos(\omega t+\phi) \\ &= V_s/2[\cos(\phi)+\cos(2\omega t+\phi)]. \end{aligned} \tag{13}$$

Applying a low pass filter, the output will be proportional to $V_s \cos(\phi)$ which provides a phase-sensitive detection of the signal.

The disadvantage of the first two options is that a bulky mechanical chopper has to be used.[65] The drawback of modulating the DC bias is that either the DC current, DC voltage, or temperature of the emitting photomixer is modulated at the lock-in frequency. This creates a parasitic distortion that can be picked up by the detector. This parasitic signal can appear as an additional DC background in the detected signal or as an additional noise which is independent of the THz signal phase.

As one of the first attempts to implement a THz transmitter/receiver system in Ref. 107, two antenna-coupled photomixers were used to test a photomixer transceiver (Fig. 23). The amplitude and phase of the THz electric-field transmission coefficient $T(\nu) = |T(\nu)|\exp[j\phi(\nu)]$ are measured as a function of time. The phase $\phi = 2\pi\nu\Delta L/c$ was determined by measuring the change in path between zeroes in the fringe pattern. Here, ΔL is the deviation from zero path difference between the two lengths of optical fiber between the beam splitter and the photomixers. The amplitude is determined by changing the zero phase distance offset d and obtaining the ratio of the fringe amplitudes with the sample in and out of the beam.

Later, Siebert et al.[83,111] performed CW THz imaging using an all-optoelectronic system using a two color Ti:sapphire laser (Fig. 24). Hyperboloidal polyethylene (PE) lenses are employed to enhance the spatial resolution of the system. Each photomixer is illuminated at 100 mW of optical power. The maximum SNR obtained at 1 THz without a sample in the beam path is 100:1. At each frequency, the spatial resolution of a THz system is defined by the spot size of the Gaussian beam on the sample which is directly proportional to the f-number of the focusing element. The f-number is given by f/d, where f is the focal length and d is the diameter of the focusing element (in case paraboloidal mirrors are used, d is the off-axis distance). For paraboloidal mirrors, f/d is always larger than $1/2$ if an object has to be brought into the focus. In contrast, hyperboloidal lenses allow for $f/d < 1/2$.

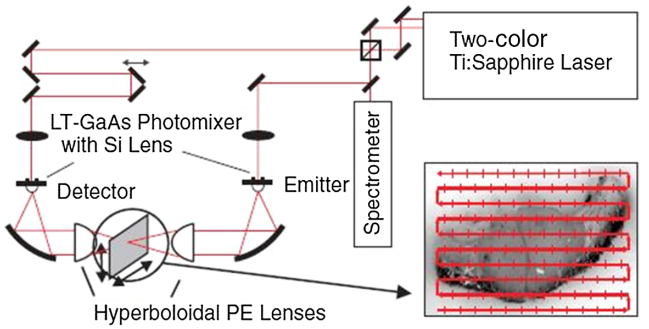

Fig. 24 Set-up of the all-optoelectronic CW THz imaging system.[83] (Copyright 2002, Institute of Physics Publishing.)

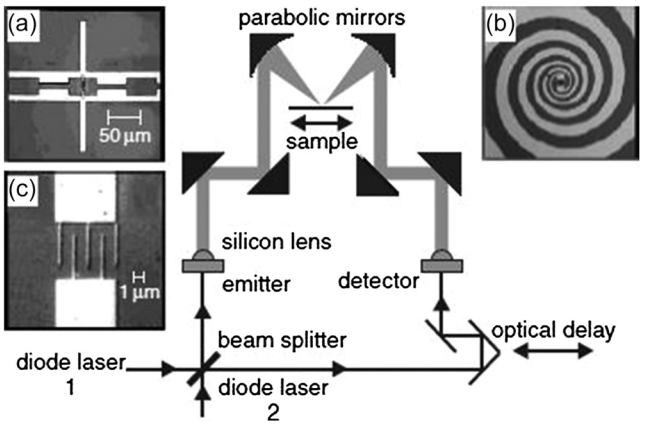

Fig. 25 CW THz schematic diagram showing combining beam splitter, optical delay line, and imaging optics. Insets: Micrographs showing: (a) resonant dipole emitter, (b) spiral detector on same scale, and (c) close-up of interdigitated finger pattern at feed point of both emitter and detector.[72] (Copyright 2004, IEE.)

Gregory et al.[71,72] introduced a CW THz imaging system that incorporates for the first time all the elements for a commercially viable system (Fig. 25). It is driven by two independent diode lasers. Two external-cavity, tunable diode lasers (TOPTICA Photonics DL100) operating at around 830 nm are combined using a 50:50 beam-splitter. The resulting two combined beams are focused onto the emitter and detector photomixers, with a delay stage in the detector beam. The optical power at the emitter (detector) was 50 mW (20 mW).

In Ref. 109, for the first time, a CW THz system with log periodic transmitter and receiver antennas on LT-GaAs substrate is reported. The system is optically driven by two laser diodes operating at a wavelength around 830 nm. As it can be seen in system schematic (Fig. 26), to overcome excess transmitter noise, the pump beam is mechanically chopped and the current is measured using a lock-in amplifier. A scanning Fabry–Perot interferometer is used to monitor the spectral mode purity. The autocorrelator monitors the optical modulation depth. An optical spectrum analyzer is used to measure the difference frequency. The SNR around 1000:1 with time constant of 300 ms and chopper speed of 1.25 KHz is achieved.

In general, efficiency of photomixing is lower than that of pulsed spectrometers. Photomixers typically contain interdigitated electrode structures[53,71,107] that are very fragile and easily experience a voltage- or temperature-induced

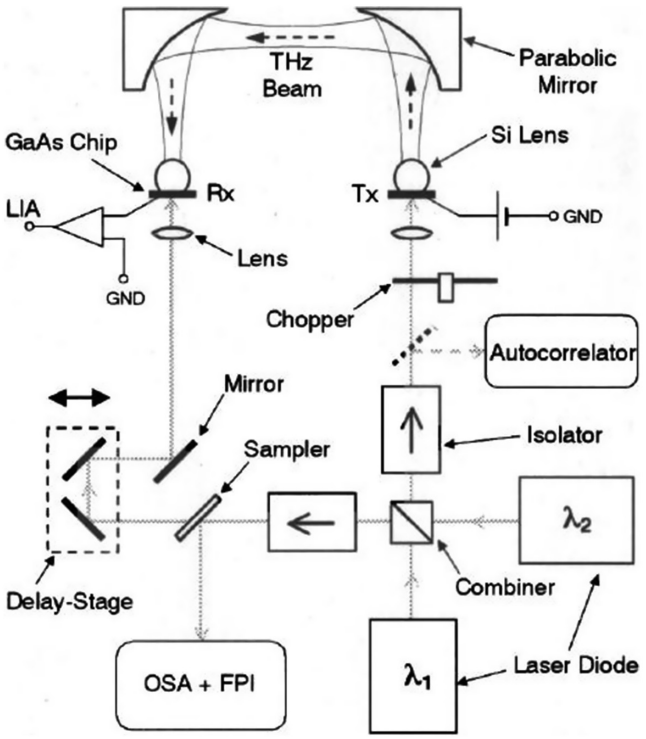

Fig. 26 CW-THz schematic diagram.[109] (Copyright 2005, Springer.)

breakdown. On the other hand, photomixers with a simple gap without interdigitated structures are considerably less efficient as a THz source. However, they are more durable and can last for years if driven at moderate voltages and optical powers. Wilk et al.[112] presented a low-cost THz spectrometer with coherent detection based on two simple and robust dipole antennas driven by two laser diodes. The spectrometer covers frequencies up to 1 THz, with a peak SNR of 40 dB for a lock-in integration time of 30 ms. The setup in Ref. 112 is used to measure the thickness of a PE wedge as a test sample. On the right (thinner) side, the thickness varies between 0.3 and 0.8 mm (Fig. 27). Figure 27 shows the measured thickness of the sample at 0.3 THz. The optical delay line was fixed during the experiment. Since the sample thickness exceeds the THz wavelength, the measured signal exhibits a sine shape. In the transmission setup, after inserting the sample, the phase of the THz signal shifts as

$$\Delta\phi = \phi_s - \phi_0 = 2\pi\nu/cd_s(n_s - 1), \tag{14}$$

where ϕ_0 and ϕ_s are phase differences in a reference (air) medium and after the insertion of the sample with thickness d_s and refractive index n_s, respectively. The sample thickness can be calculated for any pixel in the image as

$$d_s = \Delta\phi c/2\pi\nu(n_s - 1). \tag{15}$$

To extract phase information from the detected photocurrent (I_R), the measured photocurrent is normalized to its maximum ($I_R^{\max}$) first. The value of $I_R^{\max}$ can be determined via a scan with the delay line. The phases ϕ_s and ϕ_0 can be calculated as $\arccos(I_R/I_R^{\max})$ (in general, the phase has to be unwrapped).[59]

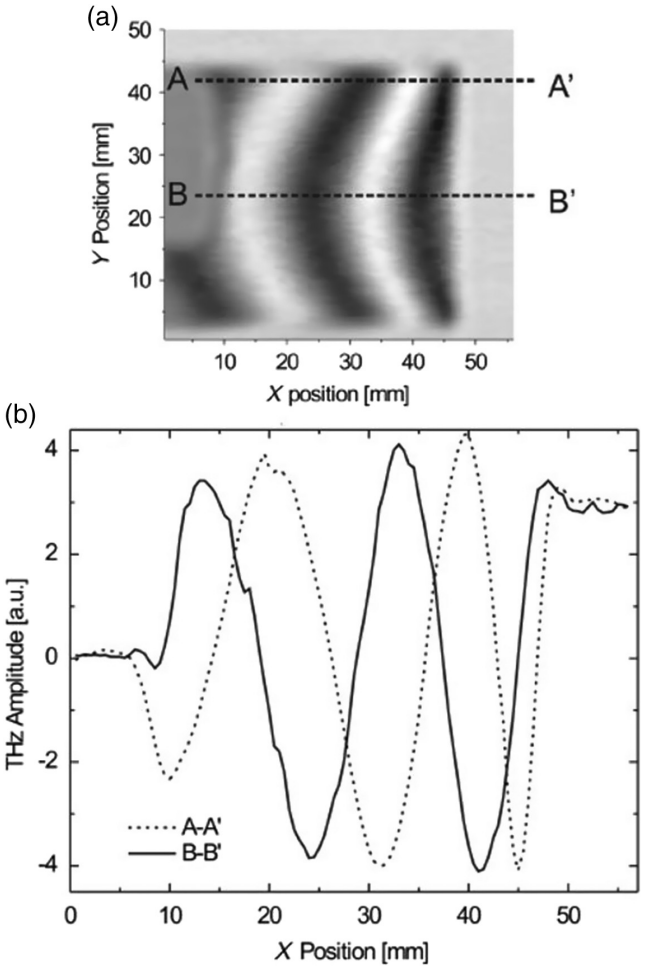

Fig. 27 (a) THz amplitude image of wedge-shaped PE and (b) its 3-D representation.[112] (Copyright 2008, Optical Society of America.)

A conventional CW THz system employs two antennas in which optical parts cause system complexity and large system size. In Ref. 110, a homodyne detection system in which a single PCA is used for both emitting and receiving the THz waves (Fig. 28). The transceiver setup reduces the system size and simplifying the alignment of optics. Since the homodyne output is considerably weak (because of the low generation efficiency in the PCA), the homodyne output is strongly affected by noise in the photocurrent. Hence, the incident laser power and bias voltage applied to the PCA must be set carefully.

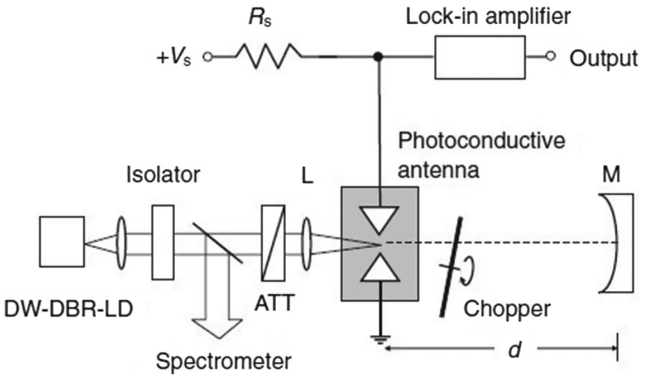

Fig. 28 Experimental setup of THz wave generator and homodyne receiver using single PCA. The emitted THz waves are reflected by concave mirror M and focused onto the same PCA.[110] (Copyright 2010, The Japan Society of Applied Physics.)

3.2 *Electro-Optic Modulator Systems*

In the measurement setup based on the electro optic modulator (EOM), a path length change of the laser wavelength in order to achieve a 2π phase variation is done electronically using an optical phase shifter.[64–67,113–119] Applying voltage in the EOM changes the refractive index and thus, the optical length of the crystal which is part of the optical path. The advantages of using optical phase modulator for phase shifting are lower measurement time rates, possible compact all-fiber set-up, and efficient use of the available laser power. This is due to the fact that there is no free space part which generates radiation loss. Figure 29 shows a setup based on EOM. Output of each of the lasers goes through a 50–50 splitter, and one of the outputs from each splitter is combined with an output from the other splitter in a 50–50 combiner. The outputs of the combiners go to the transmitter (Tx) and receiver (Rx). The phase modulator can be placed between the splitter and combiner in the transmitter or receiver path. As it can be seen in the figure only half of the power from each laser reaches to transmitter or receiver. The main drawback of this approach is that half of the laser power is lost in the second set of beam splitters. Additional laser amplifiers may be required to provide the required optical power on the photomixer. The main problem with this setup is the sensitivity of the THz phase on the optical path length. Path length jitters on the order of ~ 1 μm results in a complete loss of phase information, even though the THz amplitude is still measured accurately.[65] The other shortcomings are the significant costs for the fiber assembly and the high-voltage driver for the EOM.

The detected current in the setup in Fig. 29 is

$$I_{\text{det}}^{\text{DC}} \propto \cos(\phi_{\text{THz}} - \phi_{\text{mod}} + \phi_{\text{syst}}), \tag{16}$$

where the THz phase, ϕ_{THz} depends on the frequency difference of the two lasers and ϕ_{syst} is a function of both laser frequencies. ϕ_{syst} or the combination $\phi_{\text{THz}} + \phi_{\text{syst}}$ could be set to zero by the proper balancing of the different lengths in the system. Based on 16 optical phase shift of ϕ_{mod} is equivalent to the phase shift of the same value in the THz part of the system. The required optical delay length of the phase modulator is on the order of the optical wavelength (≈ 1 μm) for any frequency difference between the two lasers. The phase delay of the phase modulator required to

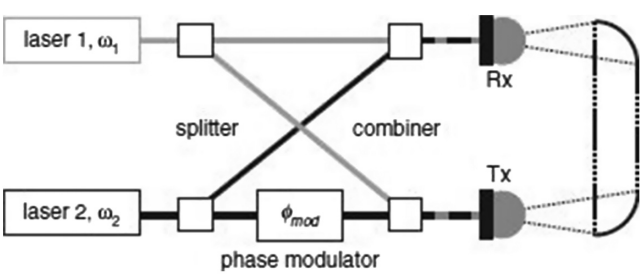

Fig. 29 General schematic of a CW THz system using optical phase modulator.[65] (Copyright 2008, IEE.)

achieve a given phase shift of the THz wave is independent of the THz frequency of the system.

In an interesting system topology in Ref. 65, optical phase modulator is used instead of the chopper. This is done by introducing an additional phase modulation (ϕ_{chop}) to ϕ_{mod}. ϕ_{chop} is change stepwise between 0 and π at the lock-in frequency, which changes stepwise the sign of the detected current $I_{\text{det}}^{\text{DC}}$ at lock-in frequency. This approach keeps the average optical power on emitter and receiver constant, and neither DC current, DC voltage nor temperature of the THz emitter are modulated. Therefore, no parasitic signal influences the detected current that reduces the noise level in the detected current. Further, the detected signal is twice as large as in the case of a mechanical chopper. Figure 30 shows the measured SNR for the mentioned three methods. The configuration with the mechanical chopper has the worst performance. The signal is 3 dB less compared to both other chopping techniques and the noise level is the highest. The signal obtained by optical phase chopping and bias modulation is identical, but the noise level achieved with the optical chopper is the lowest. The best SNR performance is obtained with chopping operation of the optical phase modulator.

To measure phase in the system in Ref. 65, multiple measurement points at each frequency have to be done. On the other hand, the system introduced in Refs. 66, 67, and 117 allows determination of both THz amplitude and phase with a single sampling point (SSP) per frequency (known as SSP method). This direct detection increases the measurement speed compared to the standard procedure. In the SSP method, THz phase is controlled by shifting the optical phase (ϕ_{mod}) of one optical beam before a beam combiner. Therefore, the phase of the optical beat signal and the emitted THz signal is shifted by the same phase ϕ_{mod}. The optical phase shift for a specified shift of the THz phase is independent of the THz frequency of the system. This allows to operate the phase modulator with the same driving voltage pattern at every THz frequency, which is the basis for method introduced in Ref. 66 in which a voltage ramp is applied to the phase modulator, which alters the THz phase by 2π [Fig. 31(a)]. This is done periodically with the desired chopping frequency. As a result, the phase of the signal detected by the receiving photomixer is periodically modulated between 0 and 2π [Fig. 31(b)]. The lock-in amplifier is locked to the control voltage of the phase modulator. Thus, the phase monitor of the lock-in amplifier does directly display the phase of the detected THz signal, enabling to detect both the THz amplitude and phase with a single measurement

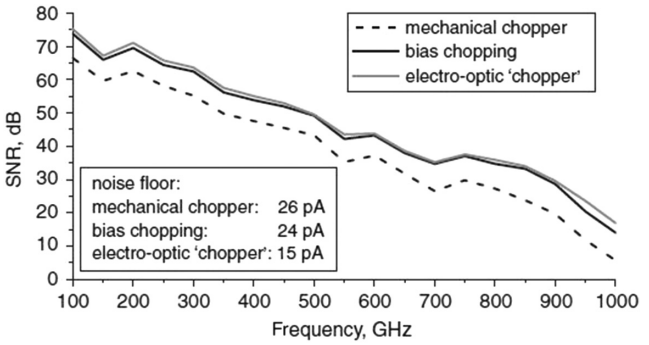

Fig. 30 SNR performance of three different chopping techniques.[65] (Copyright 2008, IEE.)

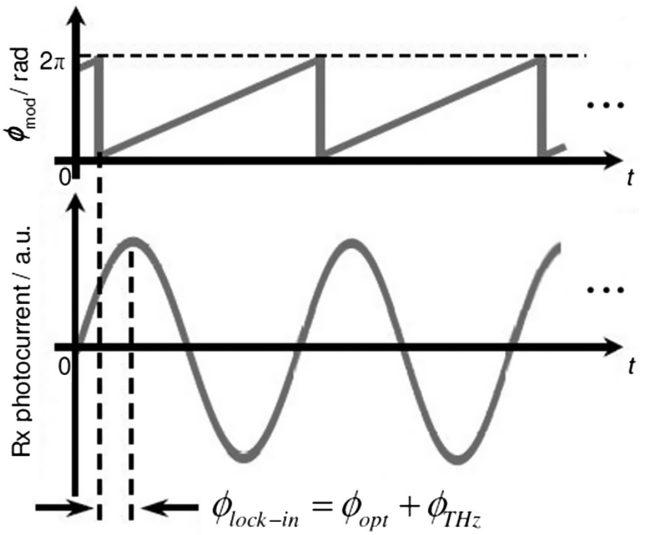

Fig. 31 Operation mode for direct phase detection. The required modulation of the THz phase is illustrated in (a), the corresponding detected signal is shown in (b).[66] (Copyright 2008, IEEE.)

point. The measured phase shift ($\phi_{\text{lock-in}}$) contains contributions due to the difference of the optical-path length in the system (ϕ_{opt}), as well as the phase accumulated in the THz part of system (ϕ_{THz}). The contribution of ϕ_{opt} is also present in any other common CW THz system, and it is eliminated with the help of calibration measurements. Figure 32 shows the measured SNR for both methods. The SNR values for the direct detection are slightly larger. The received photocurrent for both approaches is comparable, but the modulation of the transmitter bias performed for the phase-scan detection scheme induces parasitic distortions at the lock-in frequency, which leads to a higher noise level.

In Ref. 117, phase modulation ramp is used as driving signal for the lock-in detection, eliminating the need for further mechanical or electronic chopping of the THz wave. Modulation rates of 100 kHz have been employed which is approximately six orders of magnitude faster than a motor-driven translation stage. The need for a complete 2π phase shift in the modulator is shown in Fig. 33. For voltages below the equivalent of a 2π phase shift, the output waveforms

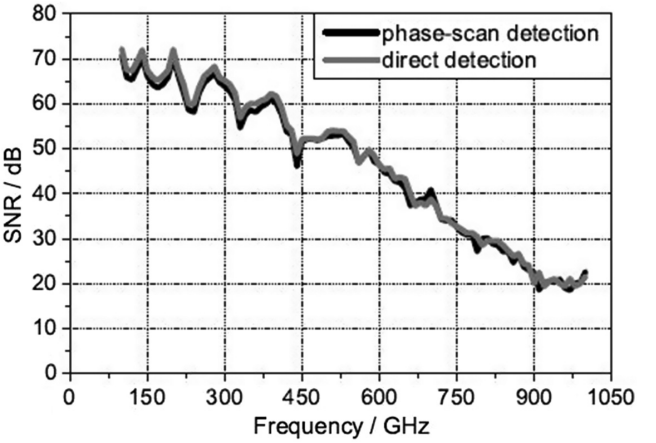

Fig. 32 SNR performance of both detection schemes.[66] (Copyright 2008, IEEE.)

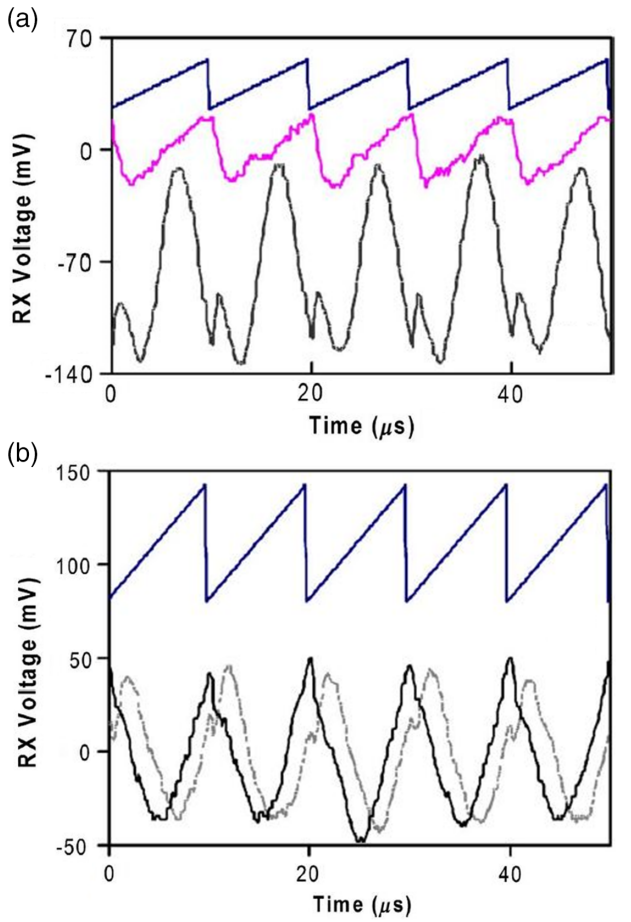

Fig. 33 THz detector voltage output versus time as a function of applied voltage to the modulator. (a) The applied voltage is 20 and 160 V (middle and bottom waveforms, respectively). The sawtooth waveform (top) illustrates the timing of the modulator voltage. Waveforms are vertically offset for clarity. (b) THz detector output for a thin card inserted (solid curve) between the THz TX and RX of Fig. 1 and removed (dashed curve).[117] (Copyright 2008, Optical Society of America.)

[Fig. 33(a)] are not complete sinusoids. For voltages that are too large [Fig. 33(b)], a waveform swing larger than one cycle is observed. The maximum scanning speed of the system in Ref. 117 is limited by the electronic bandwidth (around 400 kHz) of the THz receiver. In a classic THz imaging configuration in which the object's position is scanned in transmission mode, fast scanning system operating at 100 kHz will enable an averaging of 100 oscillations of the THz waveform with roughly 1000 pixels imaged per second. If synthetic aperture imaging methods[48] were utilized, video rate imaging would be attainable.

In Ref. 116, high speed photodiodes that are based on waveguide integrated devices are used (Fig. 34). They behave like side illuminated devices, and high absorption even for thin active layers can be achieved. High speed and high efficiency can therefore be combined. The system is completely assembled using fiber technology. The key devices emitter, receiver, lasers are telecom-related products for 1.5 μm operation. The optical power in the fiber was 30 mW at the emitter and 40 mW at the receiver. The photocurrent in the PCA (preamplified 10^8 V/A) was measured with the lock-in technique at 460-Hz modulation frequency.

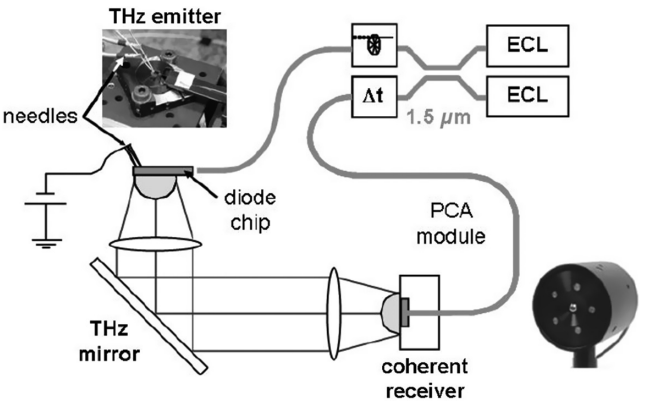

Fig. 34 Scheme of the CW THz setup[116] (Copyright 2009, OSA).

Implementations of electro-optical control setups in Refs. 66, 67, and 117 are arranged in an optical interferometer geometry and are extremely sensitive to environmental changes. In the system configurations used in these papers, the laser signals are spatially separated for wavelength selective optical phase modulation. External influences such as thermal expansion or vibrations affect the optical phase differently in the interferometer arms. This phase jitter is directly transferred into the THz phase, thus preventing high-quality measurements. The technique presented in Ref. 119 [known as wavelength selective phase modulation (WSPM)], is an in-fiber technique and realizes the speed advantage of electro optic modulation while avoiding the phase jitter normally introduced. The same phase and therefore amplitude stability as conventional systems is maintained. In WSPM, the two wavelengths remain in a single fiber. The modulation of only one wavelength is achieved by using crossed polarization for both wavelengths, together with a polarization-sensitive phase modulator (Fig. 35). Hence, if the optical phase is shifted due to environmental influences such as temperature change or mechanical stress, both wavelengths are affected identically. Thus, optical phase jitter always occurs identically on both wavelengths, and the THz phase is not affected. By applying SSP detection, high-speed measurements were demonstrated by recording a 1.5-THz spectrum with a resolution of 100 MHz in less than 24 s. This is more than 20 times faster than any previous broadband scans.[120]

The system in Ref. 115 consists of the $\lambda/4$ phase-shifted detuned dual-mode laser (DML) and an all-fiber path for the laser beams in order to increase the flexibility and compactness (Fig. 36). The optical beat signal is amplified by an erbium-doped fiber amplifier (EDFA). The amplified

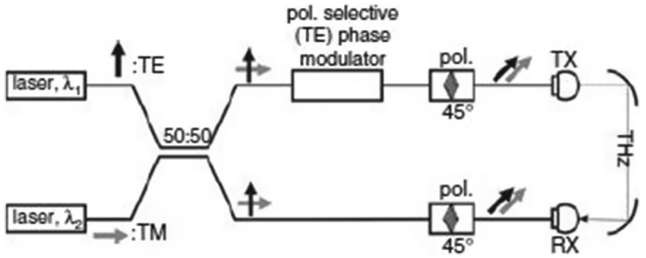

Fig. 35 Setup for in-fiber WSPM for THz phase control.[119] (Copyright 2011, IET.)

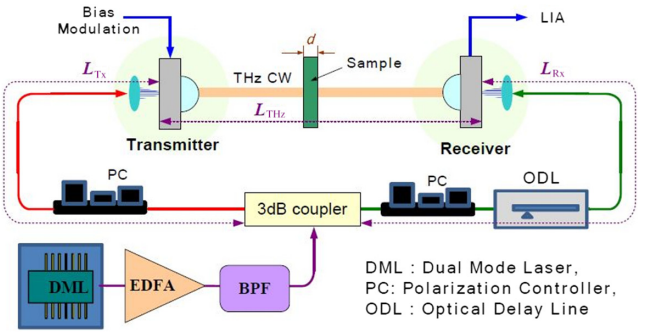

Fig. 36 Schematic diagram of a coherent homodyne CW THz system setup.[115] (Copyright 2012, OSA.)

spontaneous emission generated by the EDFA was filtered out by an optical band pass filter (BPF). The output signal from the BPF was coupled to a fiber-optic 50:50 splitter and divided into two integrated photomixer/antennas. The proposed system can be used to measure the thickness of a sample without considering the modulo 2π ambiguity.

In the setups in Refs. 67 and 113 which mentioned before phase control of THz waves in high speed, direct lock-in detection of the resulting waveform using the phase control signal as reference clock is performed. Thus, the magnitude chopping of THz wave is no longer required, and a fast THz spectroscopy system can realize millisecond-order acquisition time. However, in this scheme, the delay unbalance of the optical path or nonlinear amplitude modulation of optical signal as a parasitic effect of the electro-optic phase modulation can limit the dynamic range because the detection signal. In Ref. 114, a CW THz coherent homodyne detection system that uses push-pull electro-optic phase modulation for wide dynamic range (Fig. 37). The factors limiting detection signal quality, such as laser-induced phase noise and parasitic amplitude modulation of THz waves, are evaluated and suppressed with overall delay balance control and the push-pull phase modulation scheme. Moreover, by direct lock-in detection, fast spectroscopy and imaging measurement was demonstrated from 0.2- to 2-THz frequency range.

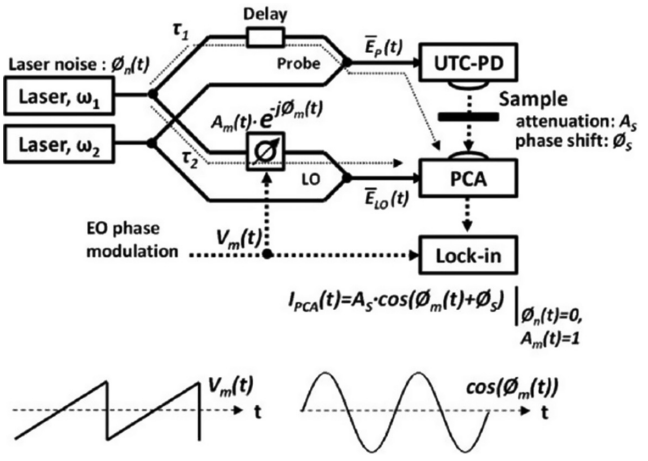

Fig. 37 CW-coherent homodyne detection system with EO phase modulation and direct lock-in detection; UTC-PD, unitraveling-carrier photodiode; PCA, photoconductive antenna.[114] (Copyright 2013, IEEE.)

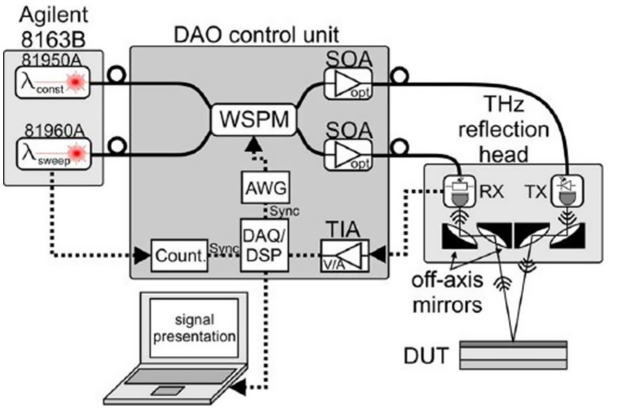

Fig. 38 Schematic of the applied CW THz system, consisting of an optical beating source (Agilent 8163B), DAO unit, and THz reflection head. The notebook is used for presentation purpose only.[118] (Copyright 2014, IEEE.)

In Ref. 118, a CW THz photomixing system (Fig. 38) which is capable of multilayer thickness measurements in reflection geometry with micrometer precision is presented which is based on Ref. 119. It also minimizes the uncertainty of the phase due to its high frequency resolution. The proposed system can replace THz time-domain systems in the field of multilayer thickness measurement due to its easier handling and much lower costs.

3.3 *Fiber Stretcher Systems*

The conventional mechanical delay stage in the THz path is rather slow because the travel of the delay line has to be comparable to or larger than the THz wavelength (i.e., 3 mm at 100 GHz). Also it requires a collimated beam in the THz path.[70,121–123] Furthermore, modulating the THz path strongly affects the standing waves, i.e., parasitic interference effects, which arise from multiple reflections of the THz beam.[68,124] Because of these standing waves, significant deviations from a cosine-like behavior of photoelectric current appears if the of the THz path is varied. On the other hand, a conventional delay stage in the path of the optical beat requires a free optical beam and thus prevents a compact all-fiber-based setup.

Fiber stretchers can be used for rapid phase modulation in the optical beam path.[70] In a typical fiber stretcher phase shifter, several tens of meters of fiber [usually polarization-maintaining (PM) fiber] are wound around a piezoelectric actuator. The piezoelectric actuator is driven by an AC voltage with an amplitude of typically 100 to 500 V. In Ref. 121, CW THz spectrometer is realized with two fiber stretchers at the two optical arms of the THz setup. Both the THz amplitude and phase are determined from 0.06 to 1.8 THz with a 1-GHz step size in less than 10 min. In their setup (Fig. 39), two DFB diode lasers are used (850 nm). Lasers are frequency stabilized by electronic feedback from a low-finesse quadrature interferometer.[59] Absolute frequency accuracy of ~100 MHz is achieved. The relative frequency resolution is in the MHz range. The laser beams are amplified at both wavelengths in a semiconductor amplifier, the output of which is once again fiber coupled. The main advantage of the dual stretcher configuration is that it reduces the sensitivity to thermal drifts and doubles the modulation amplitude compared to a single stretcher setup. Each fiber stretchers

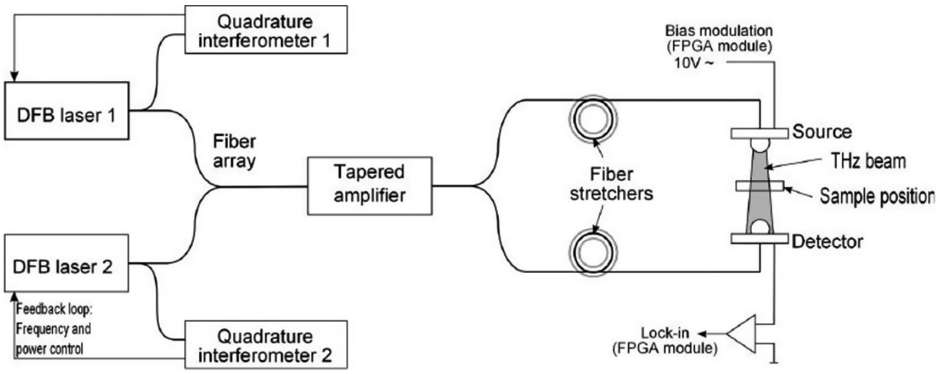

Fig. 39 Setup of the THz spectrometer for a face-to-face configuration of the two photomixers.[121] (Copyright 2011, IEEE.)

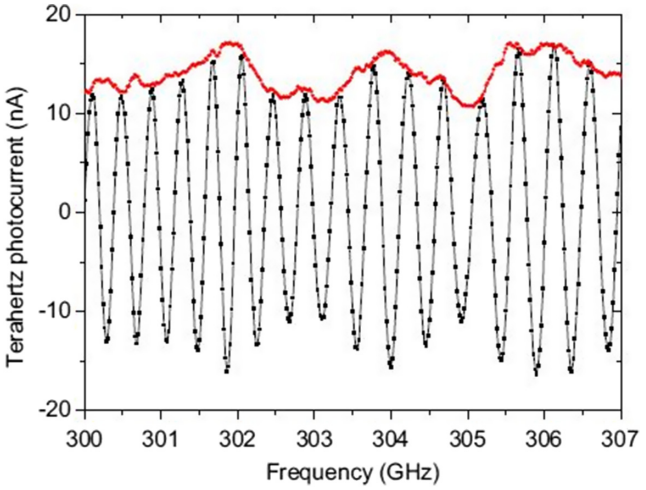

Fig. 40 THz photocurrent around $\nu = 300$ GHz measured either using the fiber stretchers (red) or a frequency-scanning method with constant path difference (black).[106] The fiber stretcher data correspond to the envelope of the oscillating pattern recorded by the frequency scan.[121] (Copyright 2011, IEEE.)

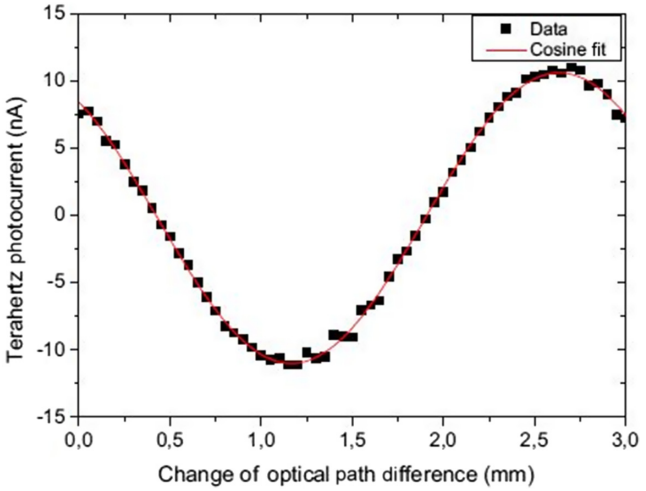

Fig. 41 Photocurrent as a function of the optical path length difference for a THz frequency of about 100 GHz.[121] (Copyright 2011, IEEE.)

consists of 60 m of PM fiber wound around a cylindrical piezo actuator which are driven with bipolar voltages of up to ± 400 V. By operating the stretchers in opposite directions, the optical path length can be changed with a twofold speed. The fiber stretchers are modulated by a continuous sinusoidal voltage to avoid switching artifacts of, e.g., a saw tooth waveform (modulation frequency is about 1 kHz).

Frequency resolution of the THz signal is not influenced by the fiber stretchers. The use of fiber stretchers yields the THz amplitude and phase for each frequency separately (Fig. 40). The main advantage of the fiber stretcher concept, compared to a delay stage in the THz beam path, is that the THz path and therefore also the unavoidable standing waves are not changed, yielding a reduced sensitivity of the amplitude and phase data to standing waves (i.e., to parasitic interferences of the THz wave). The THz photocurrent as a function of the delay length shows a "perfect" sinusoidal dependence (Fig. 41).

In Ref. 122, two identical fiber stretchers are placed in the transmitter and receiver arms. They are operated with inverted voltage with respect to each other. The receiver photocurrent is analyzed by signal averaging with a gate width of one stretcher cycle. About 240 cycles at each THz frequency step are measured, resulting in a net data acquisition rate of about 3 Hz for $f_s = 800$ Hz (f_s denotes frequency of the path difference modulation). The main advantage of signal averaging compared to a standard lock-in technique is that signal averaging does not require the receiver photocurrent to be periodic with a known reference frequency. Thus, the modulation of the optical path difference does not have to be linear in time and the maximum change does not have to be an integer multiple of the THz wavelength.

In Fig. 42, fiber stretcher voltage and the THz photocurrent are plotted as a function of time. Around the extrema of voltage, the optical path difference and thus THz photocurrent change more slowly. A sinusoidal behavior is observed in Fig. 43 in which THz photocurrent is plotted in terms of fiber stretcher voltage.

The setup in Ref. 122 is used to measure the complex refractive index of Si in transmission mode. To derive the physical properties of a sample, such as the complex index of refraction $N = n + jk$ (n and k are real and imaginary parts of refractive index), one has to compare amplitude of the THz signal (A) and phase of the THz signal (ϕ_0) measured for the sample (A_s and $\phi_{0,s}$) with those of a reference measurement (A_{ref} and $\phi_{0,\mathrm{ref}}$), which in a transmission geometry simply corresponds to a measurement on an

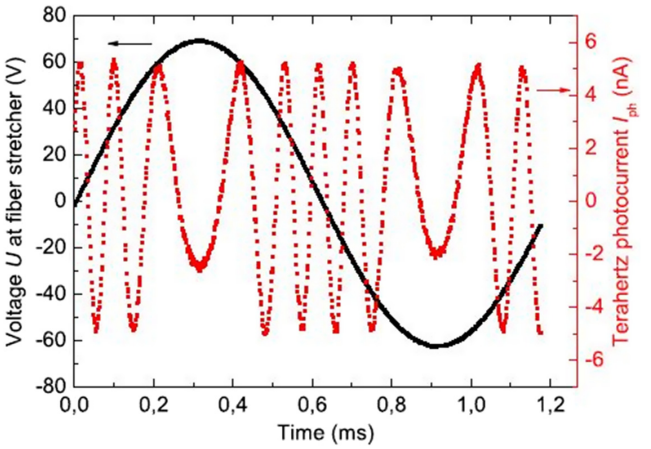

Fig. 42 Voltage at the fiber stretcher and THz photocurrent at the receiver photomixer as a function of time for a THz frequency of 600 GHz. Here, the frequency of the voltage modulation is $fs =$ 800 Hz and the photocurrent is averaged over ≈240 periods (corresponding to ≈300 ms).[122] (Copyright 2012, Optical Society of America.)

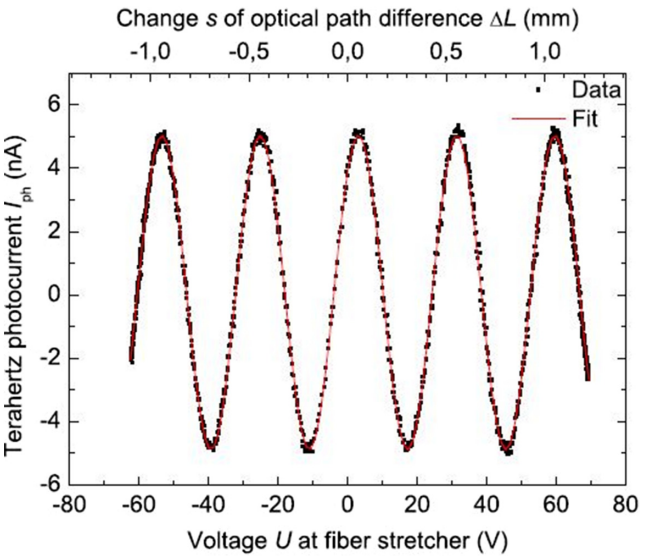

Fig. 43 The THz photocurrent (same data as in figure 443) now plotted as a function of the voltage U at the fiber stretcher, which is proportional to the change s of the optical path difference. A cosine fit with $\lambda = c/\nu \approx 500$ μm describes the data excellently (red line).[122] (Copyright 2012, Optical Society of America.)

empty aperture with the sample removed. The transmittance through the sample is $T(\nu) = [A_s(\nu)/A_{\mathrm{ref}}(\nu)]^2$, and the phase shift introduced by the sample is $\phi(\nu) = \phi_{0,s} - \phi_{0,\mathrm{ref}}(\nu) + m(\nu).2\pi$ with integer $m(\nu)$. The ambiguity in m can be resolved in a broadband measurement. If we, for instance, neglect multiple reflections within the sample of thickness d, one finds $\phi(\nu) \approx 2\pi(n-1)d\frac{\nu}{c}$, i.e., ϕ extrapolates to zero for $\nu \to 0$ and is expected to increase linearly with ν in a frequency range with constant refractive index n. Finally, knowing T and ϕ as well as the sample thickness d, one can calculate the complex index of refraction.[124]

Enhanced measurement speed and an all-fiber setup are the main advantages of the THz setup with fiber stretcher. A modulation of the optical path difference of 3 mm is obtained for a modulation frequency of ≈1 kHz. A mechanical delay stage with the same amplitude typically operates at a few hertz. A data acquisition rate of a few Hertz is achieved in Ref. 122 with averaging over about 240 cycles per frequency point. If the phase is modulated by scanning the frequency, a very similar data acquisition rate can be employed but 10 or more frequency points need to be measured to observe a phase shift of at least 2π, which yields one actual data point.[106] The fiber stretcher thus improves the measurement speed by at least an order of magnitude compared to the frequency scanning technique if the same integration times are used. It is possible to reduce the measurement time by increasing the frequency step size or to operate fiber stretchers at rates up to a few kilohertz.

Another important parameter of a THz system is the dynamic range. It is the ratio of the maximum signal to the minimum detectable signal. The amplitude of the signal depends on the optics, absorbing windows, or apertures within the THz beam, the optical power illuminating the photomixers, the bias voltage, and some other parameters. However, for equal conditions, the maximum THz amplitude is the same for the system with and without the fiber stretchers and its stability is not significantly influenced by the fiber stretchers. Other important parameters of the system are the spectral resolution and bandwidth of the system which are generally determined by the characteristics of the employed lasers.[106]

Reliable measurements of the phase require a high stability of the experimental electrical lengths. Ambient fluctuations (mostly thermal) or alignment drifts may not exceed a small fraction of the wavelength. Large wavelengths such as about 1 mm at 300 GHz thus facilitate the determination of the phase. However, fluctuations of the optical path length cannot be fully suppressed even in an air-conditioned laboratory, and phase measurements in real-world applications in a less than ideal environment are challenging, in particular, if they rely on a robust fiber-based system. These difficulties can be surpassed in ellipsometry, which measures the phase difference between different polarization states. Similar idea can be used in CW spectroscopy in the frequency domain and consider the phase difference of waves with different frequencies.

In Ref. 123, waves at three THz frequencies are generated by photomixing three different lasers (Fig. 44). The waves travel along the same path at the same time and their phases are measured simultaneously. The phase at the fixed frequency is used to monitor length changes during the measurement. The normalized phases of the two other scanning frequencies are nearly insensitive to thermal drifts. The data obtained at the reference frequency monitor the length drift of the optical path-length difference with an accuracy of about 1 to 2 μm. This can be used to self normalize the frequency dependence of the phase data measured at the scanning frequencies. The self-normalization is close to ideal because the drift correction is achieved by comparison of waves which traveled the same path at the same time, without reduction in measurement speed. This method allows for a reliable determination of the phase even in situations with large drifts such as in nonideal environmental conditions.

3.4 *Controlled Frequency Sweeping Systems*

Based on Eq. (17) changing any of the parameters, path length ΔL, or THz frequency changes the THz phase.[106,125–127]

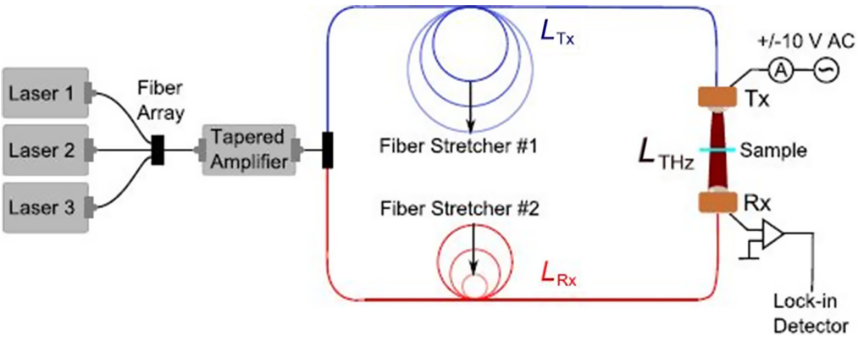

Fig. 44 Sketch of the setup with three lasers. The fiber array feeds 1/3 of the power of each laser into the amplifier. A face-to-face setup of the photomixers yields a short THz path length L_{THz}. The optical path-length difference is modulated by two fiber stretchers.[123] (Copyright 2015, AIP Publishing.)

Therefore, THz phase can equally be varied by scanning the frequency in small steps. The effect is similar to scanning an interference pattern in frequency. Phase difference is a function of the path difference ΔL and frequency. The path difference is

$$I_R \alpha E_{\mathrm{THz}} \cos(2\pi\nu\Delta L/c), \quad \Delta L = (L_s + L_{\mathrm{THz}}) - L_D, \qquad (17)$$

where L_D is traveled by the laser beat to the detector, L_s is the optical path of the laser beat to the THz source, and L_{THz} is the THz path from the source to the detector.

Phase variation in controlled frequency steps can perform as a coherent homodyne spectrometer which is a powerful tool to extract the properties of a sample in the THz region. Using a laser with a large tunability range, accurate measurements at a particular frequency can be obtained at the expense of experiment time to solve the ambiguity of modulo 2π. One advantage of this method compared to the previous approaches is that no further hardware is required, and the main disadvantage is that it needs an accurate frequency control. A frequency step has to be much smaller than the fringe pattern spacing, which in turn should be chosen much smaller than the signature of interest. One solution for high-precision frequency control is using distributed Bragg reflector diode lasers.[33,58,70,119,128,129] A second challenge arises from the large density of data points, which increases the total measurement time. A 2-THz scan with 40 MHz step size consists of more than 50,000 data points. Completing a scan in a few minutes needs lock-in times in the single-ms range.

The method has been exploited for thickness and distance measurements,[125] and for spectroscopy of solid-state samples.[58,106] Based on Eq. (17), in the case, THz beam propagates through free space (no sample), the frequency spacing of two subsequent maxima of the receiver photocurrent or zero crossings is $c/\Delta L$ (Fig. 45). By comparing the maxima or zero crossing position in measurements with and without the sample present in the THz path, we are able to measure the relative phase of the THz beam. In case, we use the maxima information, the effective frequency resolution of the phase data is $c/4\Delta L$ which is a factor two higher than the resolution of the amplitude data ($c/2\Delta L$), because only the extrema are used for the amplitude analysis (Fig. 46).

Mouret et al.[125] described the performance of the coherent homodyne spectrometer and the characterization of dielectric and semiconductor samples. The presence of the sample increases the THz path, and the period of recorded curves is affected. Assuming the refractive index of Teflon is 1.44, a thickness of 109.39 mm is measured with a standard deviation of 0.35 mm from 10 measurements. A value of 109.1 ± 0.1 mm has been obtained by using a standard mechanical micrometer. Similar information may be extracted

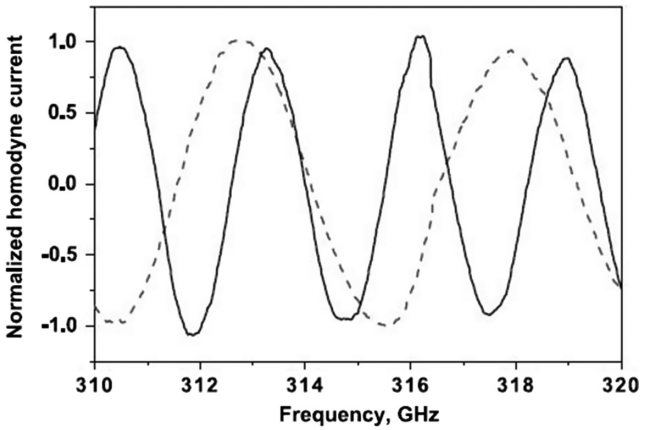

Fig. 45 Normalized homodyne signal recorded around 300 GHz with a 109.1-mm thick Teflon sample (dash line) and without (black line).[125] (Copyright 2007, Springer-Verlag.)

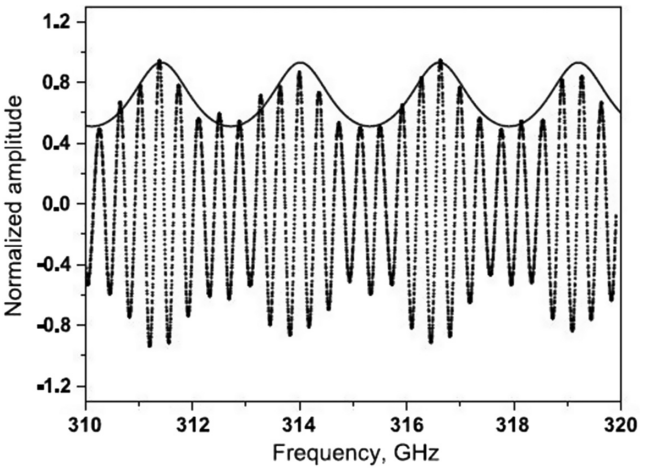

Fig. 46 Normalized homodyne signal recorded around 310 GHz with a 16.8-mm-thick high resistive silicon sample (dotted line) showing a Pèrot–Fabry effect inside the sample. The solid line is the calculated transmitted Fabry–Pèrot effect.[125] (Copyright 2007, Springer-Verlag.)

from time-domain analysis but requires the motion of a mechanical delay line and the prior knowledge of the exact position of the zero path difference. The calculated transmission amplitude of this Fabry–Pèrot effect (neglecting the absorption with constant refractive index of 3.4) is superimposed with experimental data. The analysis of the period of the homodyne signal gave a thickness of the silicon sample of 16.7 mm, in good agreement with a classical measurement. To avoid a long frequency scan, it is preferable to perform such measurements with a significant initial difference path. In this example, the period is around 0.4 GHz, the tunability of a diode laser would be sufficient to record several periods to extract the thickness of a sample or measure of distance.

CW technique offers the advantages of frequency selectivity and a much higher frequency resolution compared to time-domain techniques. Typical line widths in solid-state samples are of the order of several tens of GHz or broader. Thus, a spectral resolution of a few GHz is usually sufficient. However, a central problem for solid-state spectroscopy is that both the real and the imaginary parts of the complex refractive index $n + ik$ have to be determined reliably using amplitude and the phase of the THz radiation. The refractive index measurement method in Ref. 106 is based on scanning an interference pattern in frequency. It is based on the fact that the period of the interference pattern can be chosen to be much smaller than even the most narrow lines in a solid-state sample. It is shown that this approach is very well suited for solid-state spectroscopy, yielding precise and reliable values of real and imaginary parts of the refractive index without making use of any mechanically moving parts. The measurement setup is shown in Fig. 47.[106] The detected photocurrent I_{ph} depends on the amplitude of the THz electric field (E_{THz}), and on the phase difference $\Delta\phi$ between the THz wave and the laser beat signal [Eq. (17)]. The phase difference is varied by scanning the THz frequency. This method has the significant advantages of avoiding any mechanically moving parts and of a much higher scanning rate (up to 10 Hz, depending on the selected lock-in time, but limited by software overlap). In this case, the detected photocurrent I_{ph} oscillates with frequency (Fig. 48), and the oscillation period is set by the choice of ΔL. For reference measurement without a sample, the THz beam travels through air ($n_{\mathrm{air}} \approx 1$) independent of frequency. Thus, ΔL^{ref} is constant and the maxima are equally spaced in frequency as

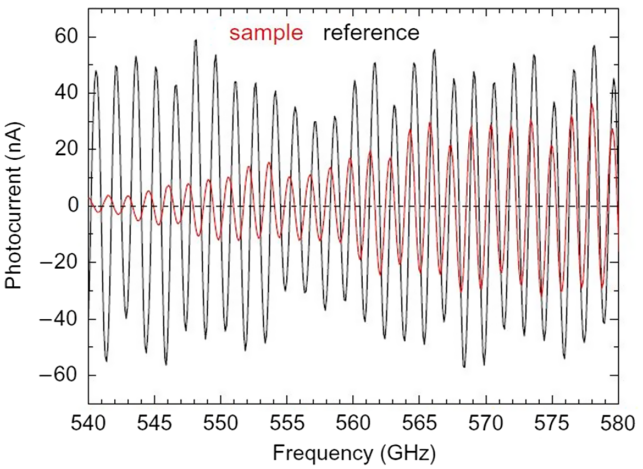

Fig. 48 An example of the detected THz photocurrent with and without the lactose sample using setup in Fig. 47. Both amplitude and phase information can be derived. The period $\Delta\nu$ of the interference pattern depends on the optical path difference ΔL. Here, $\Delta\nu \approx$ 1.5 GHz and $\Delta L \approx 0.2$ m. The suppression of the signal around 557 GHz is due to a water absorption line.[106] (Copyright 2010, IOP Institute of Physics.)

$$\nu^{\mathrm{ref}}_{\mathrm{max},m} = m\frac{c}{\Delta L^{\mathrm{ref}}}, \quad m = 1,2,3\ldots, \tag{18}$$

where ΔL_{ref} denotes the optical path difference in the case of the reference measurement.

Inserting the sample with refractive index n and thickness d in THz path changes the THz path L_{THz} by $(n - n_{\mathrm{air}})d$ (neglecting multiple reflections within the sample) which shifts the interference pattern. Figure 48 shows the detected photocurrent in the frequency range just above one of the absorption lines of lactose. The phase information can be gained from both the extrema and the zero crossings of I_{ph}, yielding a frequency resolution of the phase data of 1/4 period of the interference pattern, i.e., $c/(4 \times \Delta L)$. Thus, the spectral resolution of the phase can be adapted easily by varying the optical path difference ΔL. An enhancement of the spectral resolution, however, requires a larger density of data points, which increases the total measurement time. An interference maximum of order m occurs for $\Delta L = m \times /\nu$. Comparing reference and sample data, the refractive index can be calculated as

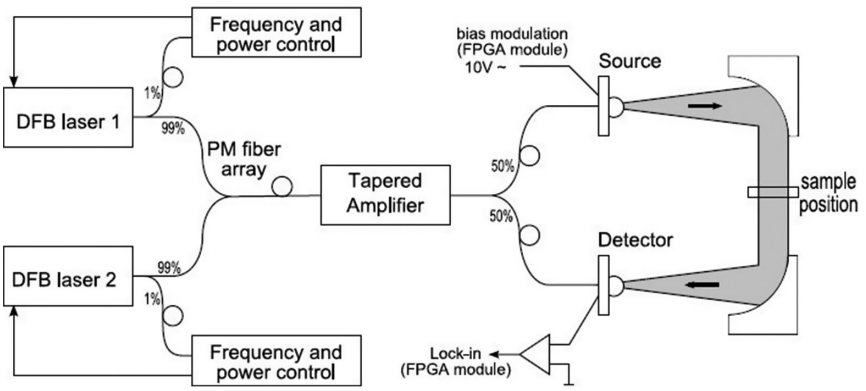

Fig. 47 Setup of the CW THz spectrometer.[106] (Copyright 2010, IOP Institute of Physics.)

$$(n - n_{\text{air}})d = \left(\frac{\nu^{\text{ref}}_{\text{max},m}}{\nu^{\text{sam}}_{\text{max},m}} - 1\right)\Delta L^{\text{ref}}, \tag{19}$$

where $\nu^{\text{ref}}_{\text{max},m}$ and $\nu^{\text{sam}}_{\text{max},m}$ are the frequencies of the maxima of order m of the reference and the sample measurement, respectively. In the reference data, the maxima are equally spaced in frequency hence, m is easily defined. Owing to the frequency dependence of the refractive index, the order of the maxima may be ambiguous in the sample data if only a narrow frequency range is explored. Determination of the absolute value of refractive index requires knowledge of the sample thickness d, which can be obtained independently from the measured amplitude. The refractive index $[n(\nu)]$ can in principle be determined entirely independently of possible fluctuations of the intensity if the zero crossings of I_{ph} are used for the determination of the phase. Precise determination of refractive index requires the stability of the frequency.

The sample also absorbs the THz light, according to its extinction coefficient $k(\nu)$. The transmittance $T(\nu)$ can be determined by comparing the envelopes of the sample data and of the reference data

$$T = \left(\frac{I^{\text{sam}}_{\text{ph}}}{I^{\text{ref}}_{\text{ph}}} - 1\right)^2, \tag{20}$$

where $I^{\text{sam}}_{\text{ph}}$ and $I^{\text{ref}}_{\text{ph}}$ are the detected photocurrents of the sample and reference data at the extrema of the respective interference patterns (the sample data are interpolated on the equally spaced frequency grid of the extrema of the reference data). Using only the extrema, the effective frequency resolution for the amplitude is $c/(2 \times \Delta L)$, well beyond the typical requirements for solid-state spectroscopy.

With the knowledge of the transmittance and the refractive index, we are able to calculate the extinction coefficient by inverting

$$T = \frac{(1 - R^2)\exp(-\alpha d}{[1 - R\,\exp(-\alpha d)]^2 + 4R\,\exp(-\alpha d)\sin^2(n2\pi\nu d/c)}, \tag{21}$$

where

$$R = \frac{(n-1)^2 + k^2}{(n+1)^2 + k^2}, \quad \alpha = 4k\pi\nu/c. \tag{22}$$

The dielectric function is obtained from

$$\epsilon_1 = n^2 - k^2, \quad \epsilon_2 = 2nk. \tag{23}$$

Measured frequency dependence of real (ϵ_1) and imaginary parts (ϵ_2) of the complex dielectric constant is shown in Fig. 49. The three absorption lines are very well resolved, whereas the additional small oscillations in ϵ_1 are artifacts of our analysis.

3.5 *Multimode Laser Mixing Systems*

In all the previously mentioned methods, mixing of two independently operating lasers has been used to generate monochromatic THz radiation. The construction of such a spectroscopic system has the advantage of generating THz beam with a narrow spectrum and tunable frequency. Another approach is using two different modes of the same laser to perform the photomixing. However, sophisticated techniques are needed for the stabilization and spatial mode matching of the two lasers. This concept is demonstrated as THz electromagnetic waves are radiated into free space

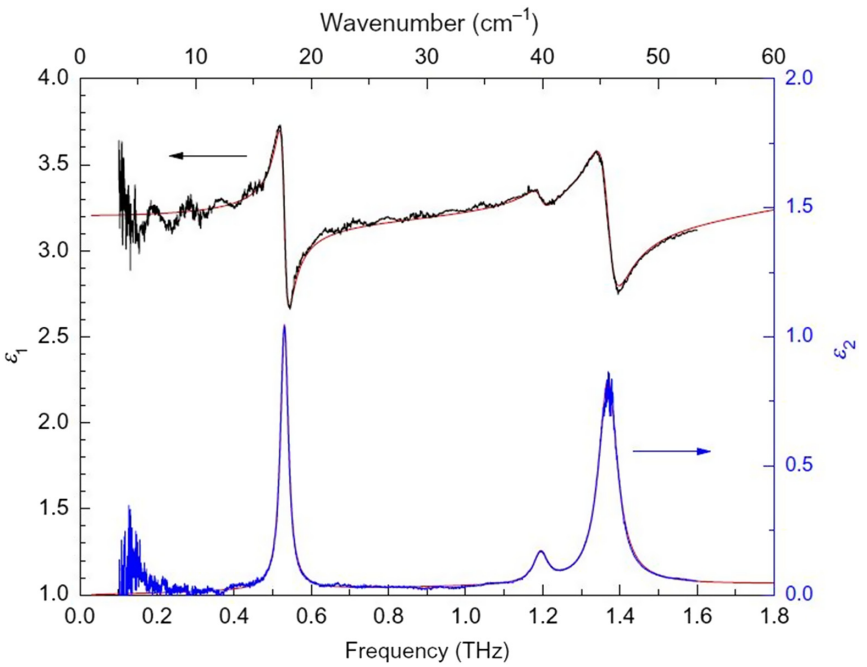

Fig. 49 Real part (black, left axis) and imaginary part (blue, right axis) of the dielectric constant of α-lactose monohydrate. The red lines depict the results of the Drude–Lorentz model based on fitting $T(\nu)$ and $n(\nu)$.[106] (Copyright 2010, IOP Institute of Physics.)

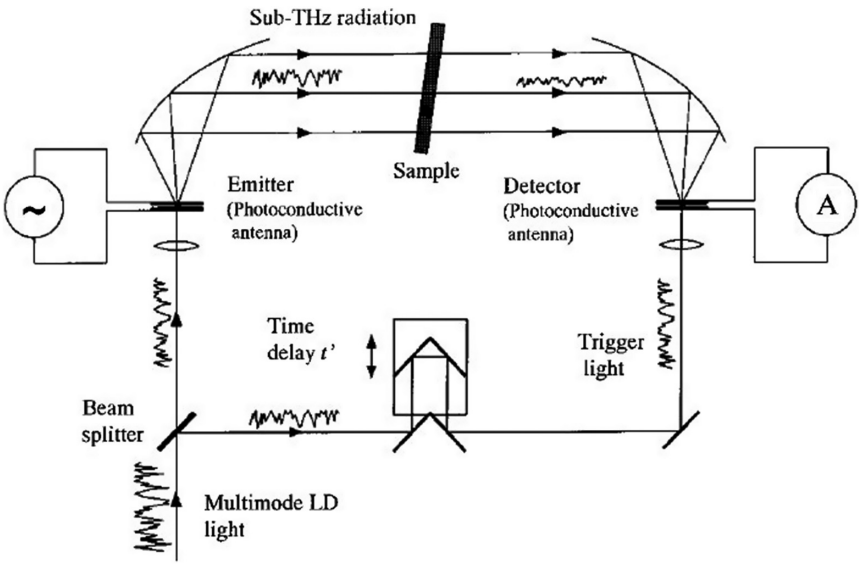

Fig. 50 Experimental configuration, which is equivalent to the TDS system except for the light source.[131] (Copyright 2000, American Institute of Physics.)

from a PCA by exciting it with a commercially available CW multimode laser diodes.[30,130] In general, a multimode laser holds many different modes and the light intensity fluctuates due to optical beats brought about by the frequency difference between modes. This random fluctuation of the light intensity can be used to produce the THz radiation. Figure 50 shows a setup that mixes modes of a laser diode to generate THz signal.[131] A PCA is irradiated by the multimode laser diode and used as an emitter. The THz radiation is collimated by an off-axial paraboloidal mirror and focused into the detector PCA by another paraboloidal mirror. A part of the multimode laser light is split by a beam splitter and introduced to the detector PCA after a time delay. The signal is modulated in a rectangular wave of 20 kHz through an emitter bias of 20 V and detected by a lock-in amplifier through a current amplifier. The sample was inserted into the THz beam path between two paraboloidal mirrors. The sample was tilted by about 10 deg to avoid the effects of standing waves between the sample surfaces and the optical elements.

Since the fluctuation of the multimode laser diode light intensity is very rapid, the current meter detects the time averaged value of the photocurrent, or the cross correlation of the electric field and the fluctuating light intensity. The reference signal $J_R(t)$, the photocurrent signal when a sample is not inserted, is expressed as

$$J_R(t) = \alpha \int_{-\infty}^{+\infty} E_R(t_0) I(t_0 - t) \mathrm{d}t_0, \tag{24}$$

where

$$E_R(t_0) = \int_{-\infty}^{+\infty} F(t_1) I(t_0 - t_1) \mathrm{d}t_1, \tag{25}$$

where $E_R(t)$ is the electric field of the radiation, α is the proportion coefficient, $I(t)$ is the light intensity, $F(t)$ is the amplitude of the impulse response function of the emitter device when the incident light and the amplitude of the THz radiation are the input and output signal, respectively. Using Fourier transformation

$$J_R(\omega) = \sqrt{2\pi}\alpha E_R(\omega) I^*(\omega) = 2\pi\alpha F(\omega)|I(\omega)|^2. \tag{26}$$

Since $I(t)$ is a real quantity, $I^*(\omega) = I(-\omega)$. In case, a sample is inserted in the THz beam path, the transmitted electric field $E_T(\omega)$ is

$$E_T(\omega) = T(\omega) E_R(\omega), \tag{27}$$

where

$$T(\omega) = |T(\omega)| \exp[-j\Phi(\omega)]. \tag{28}$$

Hence, the Fourier transformation of the photocurrent signal when the sample is inserted becomes

$$J_T(\omega) = \sqrt{2\pi}\alpha E_T(\omega) I(-\omega) = 2\pi\alpha T(\omega) F(\omega)|I(\omega)|^2. \tag{29}$$

We assume that the time average of the distribution of the laser modes causing the fluctuation of the light intensity is stationary. Therefore, it can be assumed that the power spectrum of the fluctuation is also stationary:

$$T(\omega) = J_T(\omega)/J_R(\omega). \tag{30}$$

Transmittance T and phase delay Φ of the radiation with a wavelength λ and p polarization for a solid sample with complex refractive indices $n - jk$ and thickness d can be numerically calculated as[55]

$$T(\omega) = \left| \frac{(1 - r_p^2)\sqrt{E}\, \exp(-jN)}{1 - r_P^2 E\, \exp(-2jN)} \right|^2, \tag{31}$$

$$\phi(\omega) = \arg(T) - \arg[\exp(-j2\pi d/\lambda_0) \cos\, \theta_i], \tag{32}$$

where

$$r_p = \frac{(n - jk)\cos\theta_i - \cos\theta_r}{(n - jk)\cos\theta_i + \cos\theta_r}, \tag{33}$$

$$N = 2\pi nd\cos\theta_r/\lambda_0, \tag{34}$$

$$\cos\theta_r = \frac{(n - jk)^2 - \sin^2\theta_i}{\sqrt{n - jk}}, \tag{35}$$

where θ_i is the incident angle.

The complex refractive index at each frequency can be numerically calculated from the $T(\omega)$ and $\Phi(\omega)$ obtained experimentally. One of the most popular spectroscopic systems at THz frequencies is the Fourier spectrometer which gives optical constants of both real and imaginary parts without resorting to the Kramers–Kronig analysis.[132] However, they require expensive detectors such as a bolometer cooled with liquid Helium. Time-domain THz systems are very effective but they require an expensive ultrashort-pulsed laser. On the contrary, the quasitime-domain systems are very compact and cheap and also give the equivalent data as that of Fourier spectrometer and the time-domain system. But, the SNR of this system is low compared with that of the time-domain system, which can be improved by changing the structure of the PCA.

Based on the standard photomixing theory[53] emitted THz power (P_{THz}), using a multimode laser excitation is[69]

$$P_{\mathrm{THz}} = 2\left(\frac{\eta\mu e\tau}{A}\right)^2 \cdot \sum_{i\neq j}\left(V_B^2 R_A \frac{P_i}{h\lambda_i}\frac{P_j}{h\lambda_j}\right) \times ([1 + (2\pi\nu_{ij}\tau)^2]\{1 + [1 + (2\pi\nu_{ij}R_A C)^2]\})^{-1}, \tag{36}$$

where R_A is the antenna radiation resistance, V_B is the applied bias to the emitter, A is the photomixer active area (assumed equal to the area of the focused laser spot), C is the photomixer capacitance, η is the external quantum efficiency, μ is the electron mobility, τ is the carrier lifetime. λ_i are the laser wavelengths, with corresponding laser powers P_i. ν_{ij} refers to the set of generated difference frequencies, given by $2\pi(\nu_i - \nu_j)$.

In the detector, the averaged demodulated current flow I_{THz} is given as[69]

$$I_{\mathrm{THz}} \propto \sum_{i\neq j}\alpha_{ij}E_{ij}\cos(2\pi\nu_{ij}t' + \delta_{ij}), \tag{37}$$

with

$$\alpha_{ij} = \left(V_B^2 R_A \frac{P_i}{h\lambda_i}\frac{P_j}{h\lambda_j}\right)^{1/2} \times ([1 + (2\pi\nu_{ij}\tau)^2]\{1 + [1 + (2\pi\nu_{ij}R_A C)^2]\})^{-1/2}, \tag{38}$$

where E_{ij} is the amplitude of the incident THz wave. The parameter t' is the time delay between the THz wave and the laser excitation at the detector. δ_{ij} are relative phase between modes i and j. The detected signal is only nonzero when $\nu_{\mathrm{THz}} = \nu_{ij}$, hence the cross terms in the mixer expansion have been neglected in Eq. (38) (assuming a coherent homodyne mixer with a dc output). Furthermore, in the absence of dispersion between emitter and detector, the condition $t' = 0$ coincides for each THz frequency, so that the relative phases of the emitted THz components (δ_{ij}) can be ignored. Varying t' with a time delay stage, inserted in the laser path to the receiver, allows an interferogram to be collected, in which all frequency components are in phase at $t' = 0$. A Fourier transform can be used to recover the multichannel THz power spectrum. In multimode systems, practical power limit is set by the photomixer emitters, which are commonly operated near to their breakdown point. Therefore, multiple frequencies entail an associated reduction in power for each frequency.

In Ref. 105, two laser modes are emitted from a single or combined laser cavity. The frequency fluctuation in the difference frequency is reduced by the common-mode-noise rejection effect. The frequency fluctuations common to the two modes originating from electrical, thermal, mechanical, or other sources of fluctuation are subtracted from the difference frequency even though the absolute frequencies of the two modes are drifting. One advantage of using DML is easier optical alignment. Because we do not need to align two laser beams, which is critical for photomixing efficiency.

Siebert et al.[83,111] used a dual-wavelength CW Ti:sapphire laser as the photomixing pump source. Two optical waves, with independently tunable wavelengths centered around 800 nm, were generated in the dual-wavelength laser consisting of two unidirectional, single longitudinal-mode ring cavities sharing a single Ti:sapphire gain medium which was pumped by two beams from a 5-W all-solid-state green laser (~532 nm). The two laser beams were spatially combined by using a beam-splitter and the beat frequency of the combined beam was tuned from near dc to 10 THz. Since the two beams of this dual-wavelength laser do not share the same cavity, we cannot expect a strong common-mode-rejection effect as in the case of DMLs with a single cavity. However, the dual-cavity laser with single gain media has the obvious advantage in the system simplicity and a wide difference-frequency tunability which is free from the instability due to the mode interaction in close vicinity.

In Ref. 77, a microchip laser with two longitudinal modes is used to pump a PCA to generate an ultranarrowband THz radiation. The microchip laser consisted of a Nd:YVO4 chip (operating wavelength ~1064 nm) with 0.5 mm length.

The laser mode frequency fluctuates due to the temperature change, power fluctuations of the pump laser, and mechanical vibration. When the two laser modes oscillate in the same cavity, the direction and amplitude of the frequency shift are similar for the two modes. Therefore, the difference beat frequency does not change as much as the original laser modes do. The common-mode rejection ratio (CMRR) as the ratio of frequency shift of the laser mode to the shift in the difference frequency:

$$\mathrm{CMRR} = \frac{\sqrt{0.5(\Delta^2 f_1 + \Delta^2 f_2)}}{|f_1 - f_2|}. \tag{39}$$

When there is no effect of material dispersion and mode interaction, Eq. (39) gives us the ratio of the optical frequency and the beat frequency due to the linear relationship between f_1 and f_2. In Ref. 77, the linewidth of the beat frequency of the two modes is narrower than that of individual laser modes because of the common-mode rejection effect for the two modes oscillating in the same cavity.

External cavity dual-mode semiconductor lasers have been realized in a variety of methods, such as those with

a double grating,[56,133] grating-lens,[134] grating-double-slit,[134] grating-double-stripe-mirror[73,135] configurations, etc.

The DML excitation for photomixing is preferable to that by two independent lasers since the system can be more compact and the difference frequency stability is improved by the common-mode rejection effect. Although the difference frequency stability of dual-mode semiconductor lasers reported was not good enough (mainly due to the nonoptimized conditions), there is a great potential in THz photomixing systems with dual-mode semiconductor lasers with the external cavity because of the wide-tunability and compactness of the system.

4 Conclusions

Each of the CW and pulsed THz systems have unique advantages and shortcomings that must be carefully considered when they are being used for different applications. In general, time-domain systems are relatively more complex and expensive but they provide information that is not accessible in a CW system. In the case, this information is imprecise or too difficult to interpret, the advantages offered by a time-domain system quickly disappear. The main contrast between the two modalities is between simplicity and adaptability. In many applications, the additional information is unnecessary, and a pulsed system has no advantage and in others such information may become useful.

Among many THz wave sources such as free electron lasers, BWO tubes, electronic sources, and THz lasers; a THz photomixer is the cheap, simple, and quite prospective option. Present-day photomixers have undergone a considerable development over the past two decades and have come a long way from the initial laboratory setups to compact and portable spectrometers that are already employed in industrial implementations.

Due to research and developments during the last two decades in THz domain, devices such as lasers, THz transmitters, and detectors and also detection techniques have sufficiently matured to take the step out of the lab and into "real-world" applications. Here, we reviewed different system architectures which have been developed based on the photomixing sources and detectors. Each system has its advantages, and shortcomings which have to be carefully considered for each specific application.

The biggest technological challenge that photoconductive emitters face these days is their cost-effective large-scale production viability. Low-temperature GaAs is still the most widely used material for photoconductive devices; however, its fabrication has two major disadvantages. First, the semiconductor properties are difficult to reproduce, even when grown under the same nominal conditions. Second, its growth requires being performed in molecular-beam-epitaxy machines, which is an expensive method. The development of compact and on-chip THz imaging and spectroscopy systems will be a driver for the further development of photoconductive THz devices.

References

1. R. A. Lewis, "A review of terahertz sources," *J. Phys. D Appl. Phys.* **47**, 374001 (2014).
2. M. Asada, S. Suzuki, and N. Kishimoto, "Resonant tunneling diodes for sub-terahertz and terahertz oscillators," *Jpn. J. Appl. Phys.* **47**(6R), 4375–4384 (2008).
3. J. Yun, D. Yoon, and J.-S. Rieh, "Compact solid-state electronic terahertz devices and circuits," in *Terahertz Biomedical Science and Technology*, J.-H. Son, Ed., CRC Press, Taylor & Francis Group, Florida, pp. 82–107 (2014).
4. D. W. Porterfield, "High-efficiency terahertz frequency triplers," in *IEEE/MTT-S Int. Microwave Symp.*, IEEE, pp. 337–340 (2007).
5. D. H. Auston, K. P. Cheung, and P. R. Smith, "Picosecond photoconducting Hertzian dipoles," *Appl. Phys. Lett.* **45**(3), 284–286 (1984).
6. N. M. Burford and M. O. El-Shenawee, "Review of terahertz photoconductive antenna technology," *Opt. Eng.* **56**(1), 010901 (2017).
7. F. Wang et al., "A high-efficiency regime for gas-phase terahertz lasers," *Proc. Natl. Acad. Sci. U. S. A.* **115**(26), 6614–6619 (2018).
8. P. Tan et al., "Terahertz radiation sources based on free electron lasers and their applications," *Sci. China Inf. Sci.* **55**(1), 1–15 (2012).
9. G. Chen et al., "Terahertz-wave imaging system based on backward wave oscillator," *IEEE Trans. Terahertz Sci. Technol.* **2**(5), 504–512 (2012).
10. C. Weiss et al., "Tuning characteristics of narrowband THz radiation generated via optical rectification in periodically poled lithium niobate," *Opt. Express* **8**, 497–502 (2001).
11. J. Dai, J. Liu, and X.-C. Zhang, "Terahertz wave air photonics: terahertz wave generation and detection with laser-induced gas plasma," *IEEE J. Sel. Top. Quantum Electron.* **17**(1), 183–190 (2011).
12. B. S. Williams, "Terahertz quantum-cascade lasers," *Nat. Photonics* **1**, 517–525 (2007).
13. C. M. Armstrong, "The truth about terahertz," *IEEE Spectrum* **49**, 36–41 (2012).
14. F. Alves et al., "Bi-material terahertz sensors using metamaterial structures," *Opt. Express* **21**(11), 13256–13271 (2013).
15. F. Alves et al., "Microelectromechanical systems bimaterial terahertz sensor with integrated metamaterial absorber," *Opt. Lett.* **37**(11), 1886–1888 (2012).
16. Y. Cai et al., "Coherent terahertz radiation detection: direct comparison between free-space electro-optic sampling and antenna detection," *Appl. Phys. Lett.* **37**(4), 444 (1998).
17. F. Sizov, "Terahertz radiation detectors: the state-of-the-art," *Semicond. Sci. Technol.* **33**, 123001 (2018).
18. M. A. B. Saucedo, "Signal and data processing for terahertz imaging," PhD Thesis, University of Manchester (2014).
19. N. Karpowicz et al., "Comparison between pulsed terahertz time-domain imaging and continuous wave terahertz imaging," *Semicond. Sci. Technol.* **20**, S293–S299 (2005).
20. J. L. Johnson, T. D. Dorney, and D. M. Mittleman, "Interferometric imaging with terahertz pulses," *IEEE J. Sel. Top. Quantum Electron* **7**(4), 592–599 (2001).
21. J. O'Hara and D. Grischkowsky, "Quasi-optic synthetic phased-array terahertz imaging," *J. Opt. Soc. Am. B* **21**, 1178–1191 (2004).
22. S. Matsuura and H. Ito, *Terahertz Optoelectronics*, Springer, Berlin (2005).
23. J. F. Federici et al., "THz imaging and sensing for security applications—explosives, weapons and drugs," *Semiconductor Sci. Technol.* **20**, S266 (2005).
24. H. Liu et al., "Detection and identification of explosive RDX by THz diffuse reflection spectroscopy," *Opt. Express* **14**, 415–423 (2006).
25. D. Banerjee et al., "Diagnosing water content in paper by terahertz radiation," *Opt. Express* **16**, 9060–9066 (2008).
26. J. P. Dougherty, G. D. Jubic, and W. L. Kiser, "Terahertz imaging of burned tissue," *Proc. SPIE* **6472**, 64720N (2007).
27. M. Schirmer et al., "Biomedical applications of a real-time terahertz color scanner," *Biomed. Opt. Express* **1**(2), 354–366 (2010).
28. N. N. Zinovev et al., "Identification of tooth decay using terahertz imaging and spectroscopy," in *Twenty Seventh Int. Conf. Infrared and Millimeter Waves* (2002).
29. S. Matsuura, M. Tani, and K. Sakai, "Generation of coherent terahertz radiation by photomixing in dipole photoconductive antennas," *Appl. Phys. Lett.* **70**, 559–561 (1997).
30. O. Morikawa, M. Tonouchi, and M. Hangyo, "Sub-THz spectroscopic system using a multimode laser diode and photoconductive antenna," *Appl. Phys. Lett.* **75**, 3772 (1999).
31. S. Nellen et al., "Recent progress of continuous-wave terahertz systems for spectroscopy, non-destructive testing, and telecommunication," *Proc. SPIE* **10531**, 105310C (2018).
32. E. F. Pliński, "Terahertz photomixer," *Bull. Pol. Acad. Sci.* **58**, 463 (2010).
33. M. Scheller, K. Baaske, and M. Koch, "Multifrequency continuous wave terahertz spectroscopy for absolute thickness determination," *Appl. Phys. Lett.* **96**, 151112 (2010).
34. M. Scheller and M. Koch, "Terahertz quasi time domain spectroscopy," *Opt. Express* **17**, 17723–17733 (2009).
35. K. Kawase, "Terahertz imaging for drug detection and large-scale integrated circuit inspection," *Opt. Photonics News* **15**(10), 34–39 (2004).
36. C. Jordens et al., "Evaluation of the leaf water status by means of the permittivity at terahertz frequencies," *J. Biol. Phys.* **35**, 255–264 (2009).
37. T. Yasui et al., "Terahertz paint meter for non contact monitoring of thickness and drying progress in paint film," *Appl. Opt.* **44**, 6849–6856 (2005).

38. A. J. L. Adam et al., "Terahertz imaging of hidden paint layers on canvas," *Opt. Express* **17**, 3407–3416 (2009).
39. K. Fukunaga et al., "Terahertz spectroscopy for art conservation," *IEICE Electron. Express* **4**, 258–263 (2007).
40. C. Jansen et al., "Terahertz imaging: applications and perspectives," *Appl. Opt.* **49**(19), E48–E57 (2010).
41. N. Krumbholz et al., "Monitoring polymeric compounding processes inline with THz time-domain spectroscopy," *Polym. Test.* **28**, 30–35 (2009).
42. C. D. Stoik, M. J. Bohn, and J. L. Blackshire, "Nondestructive evaluation of aircraft composites using transmissive terahertz time domain spectroscopy," *Opt. Express* **16**, 17039–17051 (2008).
43. K. Yamamoto et al., "Degradation diagnosis of ultrahigh-molecular weight polyethylene with terahertz-time-domain spectroscopy," *Appl. Phys. Lett.* **85**, 5194–5196 (2004).
44. H. Wu and M. Khan, "THz spectroscopy: an emerging technology for pharmaceutical development and pharmaceutical process analytical technology (PAT) applications," *J. Mol. Struct.* **1020**, 112–120 (2012).
45. K. Ajito, J. Y. Kim, and H. J. Song, "Continuous wave terahertz spectroscopy system designed for medical field," *Feature Articles: R&D on Devices Using Life-Assist Technologie* (2015).
46. W. L. Chan, J. Deibel, and D. M. Mittleman, "Imaging with terahertz radiation," *Rep. Prog. Phys.* **70**, 1325–1379 (2007).
47. Y. Ayesha, "Imagerie terahertz 2D et 3D: application pour l'étude des materiaux du pat- rimoine culturel," PhD Thesis, Queensland University of Technology (2011).
48. A. Bandyopadhyay et al., "Terahertz interferometric and synthetic aperture imaging," *J. Opt. Soc. Am. A* **23**, 1168–1178 (2006).
49. D. B. Bennett et al., "Terahertz sensing in corneal tissues," *J. Biomed. Opt.* **16**(5), 057003 (2011).
50. L. Yu et al., "The medical application of terahertz technology in non-invasive detection of cells and tissues: opportunities and challenges," *RSC Adv.* **9**, 9354–9363 (2019).
51. M. Bessou et al., "Three-dimensional terahertz computed tomography of human bones," *Appl. Opt.* **51**(28), 6738–6744 (2012).
52. A. Brahm et al., "Volumetric spectral analysis of materials using terahertz-tomography techniques," *Appl. Phys. B* **100**(1), 151–158 (2010).
53. E. R. Brown et al., "Photomixing up to 3.8 THz in low-temperature-grown GaAs," *Appl. Phys. Lett.* **66**, 285 (1995).
54. J.-P. Caumes et al., "Terahertz tomographic imaging of XVIIIth dynasty Egyptian sealed pottery," *Appl. Opt.* **50**(20), 3604–3608 (2011).
55. R. E. Collin, *Field Theory of Guided Waves*, McGraw-Hill, New York (1960).
56. A. Tunnermann et al., "Continuously tunable external-cavity diode laser with a double-grating arrangement," *Opt. Lett.* **22**, 390–392 (1997).
57. C. L. K. Dandolo et al., "Terahertz frequency modulated continuous wave imaging advanced data processing for art painting analysis," *Opt. Express* **26**(5), 5358–5367 (2018).
58. J. R. Demers, R. T. Logan, Jr., and E. R. Brown, "An optically integrated coherent frequency-domain THz spectrometer with signal-to-noise ratio up to 80 dB," in *Int. Topical Meeting Microwave Photonics Tech. Dig.* (2007).
59. A. J. Deninger et al., "Precisely tunable continuous-wave terahertz source with interferometric frequency control," *Rev. Sci. Instrum.* **79**(4), 044702 (2008).
60. S. S. Dhillon et al., "The 2017 terahertz science and technology roadmap," *J. Phys. D Appl. Phys.* **50**, 043001 (2017).
61. H. Elayan et al., "Terahertz communication: the opportunities of wireless technology beyond 5G," in *Int. Conf. Adv. Commun. Technol. Networking (CommNet)* (2018).
62. B. Ferguson et al., "T-ray computed tomography," *Opt. Lett.* **27**(15), 1312–1314 (2002).
63. Gentec, https://www.gentec-eo.com.
64. T. Göbel, "Systeme, Verfahren und Komponenten zur hochaufl ösenden Dauerstrich-Terahertz- Spektroskopie," PhD Thesis, University of Darmstadt, Germany (2010).
65. T. Göbel et al., "Continuous-wave terahertz system with electro-optical terahertz phase control," *Electron. Lett.* **44**(14), 863–864 (2008).
66. T. Göbel et al., "Direct phase detection in continuous-wave photomixing THz systems," in *21st Annu. Meeting IEEE Lasers and Electro-Opt. Soc.* (2008).
67. T. Göbel et al., "Single-sampling-point coherent detection in continuous-wave photomixing terahertz systems," *Electron. Lett.* **45**(1), 65–66 (2009).
68. B. P. Gorshunov et al., "Terahertz BWO spectroscopy of conductors and superconductors," *Quantum Electron.* **37**, 916 (2007).
69. I. S. Gregory et al., "Multi-channel homodyne detection of continuous-wave terahertz radiation," *Appl. Phys. Lett.* **87**, 034106 (2005).
70. I. S. Gregory et al., "Analysis of photomixer receivers for continuous-wave terahertz radiation," *Appl. Phys. Lett.* **91**(15), 154103 (2007).
71. I. S. Gregory et al., "Continuous wave terahertz system with a 60 dB dynamic range," *Appl. Phys. Lett.* **86**, 204104 (2005).
72. I. S. Gregory et al., "Phase sensitive continuous wave THz imaging using diode lasers," *Electron. Lett.* **40**(2), 143 (2004).
73. P. Gu et al., "Generation of coherent cw-terahertz radiation using a tunable dual-wavelength external cavity laser diode," *Jpn. J. Appl. Phys.* **38**, L1246–L1248 (1999).
74. J. P. Guillet et al., "Art painting diagnostic before restoration with terahertz and millimeter waves," *J. Infrared Millimeter Terahertz Waves* **38**(4), 369–379 (2017).
75. J. Guillet et al., "Frequency modulated continuous wave terahertz imaging for art restoration," in *Proc. IEEE Conf. Infrared, Millimeter, and Terahertz Waves* (2016).
76. P. Hillger et al., "Low-cost 0.5 THz computed tomography based on silicon components," in *42nd Int. Conf. Infrared, Millimeter, and Terahertz Waves (IRMMW-THz)*, IEEE, pp. 1–2 (2017).
77. M. Hyodo et al., "Generation of millimetre-wave generation using a dual-longitudinal mode microchip laser," *Electron. Lett.* **32**, 1589–1591 (1996).
78. Ino, https://www.ino.ca.
79. C. S. Jöseph et al., "Imaging of ex vivo nonmelanoma skin cancers in the optical and terahertz spectral regions optical and terahertz skin cancers imaging," *J. Biophotonics* **7**(5), 295–303 (2014).
80. E. Jung et al., "Quantitative analysis of water distribution in human articular cartilage using terahertz time-domain spectroscopy," *Biomed. Opt. Express* **3**(5), 1110–1115 (2012).
81. M. Xu, K. A. Niessen, and A. G. Markelz, "Terahertz optical measurements of correlated motions with possible allosteric function," *Biophys. Rev.* **7**(2), 201–216 (2015).
82. K. Kawase, Y. Ogawa, and Y. Watanabe, "Non-destructive terahertz imaging of illicit drugs using spectral fingerprints," *Opt. Express* **11**, 2549–2554 (2003).
83. K. J. Siebert et al., "All-optoelectronic continuous wave THz imaging for biomedical applications," *Phys. Med. Biol. J.* **47**, 3743–3748 (2002).
84. T. Kleine-Ostmann et al., "Continuous-wave THz imaging," *Electron. Lett.* **37**(24), 1461 (2001).
85. L. Öhrström et al., "Terahertz imaging of ancient mummies and bone," *Am. J. Phys. Anthropol.* **142**(3), 497–500 (2010).
86. S. Wang and X.-C. Zhang, "Tomographic imaging with a terahertz binary lens," *Appl. Phys. Lett.* **82**(12), 1821–1823 (2003).
87. J. Takayanagi et al., "High-resolution time-of-flight terahertz tomography using a femtosecond fiber laser," *Opt. Express* **17**(9), 7533–7539 (2009).
88. P. Tewari et al., "*In vivo* terahertz imaging of rat skin burns," *J. Biomed. Opt.* **17**(4), 040503 (2012).
89. L. Rong et al., "Terahertz in-line digital holography of human hepatocellular carcinoma tissue," *Sci. Rep.* **5**, 8445 (2015).
90. B. Li et al., "Application of continuous-wave terahertz computed tomography for the analysis of chicken bone structure," *Opt. Eng.* **57**(2), 023105 (2018).
91. E. Abraham et al., "Refraction losses in terahertz computed tomography," *Opt. Commun.* **283**(10), 2050–2055 (2010).
92. I. Abdulhalim and M. Ney, "Ultrahigh polarimetric image contrast enhancement for skin cancer diagnosis using InN plasmonic nanoparticles in the terahertz range," *J. Biomed. Opt.* **20**(12), 125007 (2015).
93. Z. D. Taylor et al., "THz and mm-wave sensing of corneal tissue water content: in vivo sensing and imaging results," *IEEE Trans. Terahertz Sci. Technol.* **5**, 184–196 (2015).
94. H. P. Chan et al., "Feasibility of terahertz reflectometry for discrimination of human early gastric cancers," *Biomed. Opt. Express* **6**, 1398–1406 (2015).
95. TeraView, https://teraview.com.
96. Siklu Communication Ltd., https://www.siklu.com/press-release/thzradio-link/.
97. Orbis, https://www.bvdinfo.com.
98. Advantest, https://www.advantest.com.
99. MenloSystems, https://www.menlosystems.com.
100. Microtech, http://mtinstruments.com.
101. TeraSense, http://terasense.com.
102. Toptica, https://www.toptica.com.
103. Traycer, https://www.traycer.com.
104. D. Saeedkia, *Handbook of Terahertz Technology for Imaging, Sensing and Communications*, International Series of Monographs on Physics, Woodhead Publishing Series in Electronic and Optical Materials, Number 34, WP Woodhead Publishing (2013).
105. M. Tani et al., "Generation of terahertz radiation by photomixing with dual- and multiple-mode lasers," *Semicond. Sci. Technol.* **20**, S151 (2005).
106. A. Roggenbuck et al., "Coherent broadband continuous-wave terahertz spectroscopy on solid-state samples," *New J. Phys.* **12**, 043017 (2010).
107. S. Verghese et al., "Generation and detection of coherent terahertz waves using two photomixers," *Appl. Phys. Lett.* **73**(26), 3824–3826 (1998).
108. S. Verghese and K. A. McIntosh, "Quasi-optical transceiver having an antenna with time varying voltage," Patent US 6,348,683 (2002).
109. R. Mendis et al., "Coherent generation and detection of continuous terahertz waves using two photomixers driven by laser diodes," *Int. J. Infrared Millimeter Waves* **26**(2), 201–207 (2005).

110. K. Murasawa and T. Hidaka, "Generation and homodyne detection of continuous terahertz waves using single photoconductive antenna," *Jpn. J. Appl. Phys.* **49**, 122401 (2010).
111. K. J. Siebert et al., "Continuous-wave all-optoelectronic terahertz imaging," *Appl. Phys. Lett.* **80**(16), 3003–3005 (2002).
112. R. Wilk et al., "Continuous wave terahertz spectrometer as a noncontact thickness measuring device," *Appl. Opt.* **47**(16), 3023–3026 (2008).
113. J. Y. Kim et al., "Continuous- wave coherent homodyne detection with balanced electro-optical phase modulation," in *Proc. Int. Conf. Infrared Millimeter Waves* (2012).
114. J. Y. Kim et al., "Continuous-wave THz homodyne spectroscopy and imaging system with electro-optical phase modulation for high dynamic range," *IEEE Trans. Terahertz Sci. Technol.* **3**(2), 158–164 (2013).
115. H. C. Ryu et al., "Simple and cost-effective thickness measurement terahertz system based on a compact 1.55 μm $\lambda/4$ phase-shifted dual-mode laser," *Opt. Express* **20**(23), 25990–25999 (2012).
116. B. Sartorius et al., "Continuous wave terahertz systems exploiting 1.5 μm telecom technologies," *Opt. Express* **17**(17), 15001–15007 (2009).
117. A. M. Sinyukov et al., "Rapid-phase modulation of terahertz radiation for high-speed terahertz imaging and spectroscopy," *Opt. Lett.* **33**(14), 1593–1595 (2008).
118. D. Stanze et al., "Multilayer thickness determination using continuous wave THz spectroscopy," *IEEE Trans. Terahertz Sci. Technol.* **4**(6), 696–701 (2014).
119. D. Stanze et al., "Single-sampling-point coherent detection in continuous-wave photomixing terahertz systems," *Electron. Lett.* **45**(1), 65–66 (2011).
120. "Teraview: CW Spectra 400—Continuous Wave (CW) terahertz spectrometer with imaging capability," https://www.4science.net/goods/proc/attachDownload.do?mtf_no=52009 (2010).
121. A. Roggenbuck et al., "A fast CW-THz spectrometer using fiber stretchers," in *Proc. IRMMW-THz Conf.* (2011).
122. A. Roggenbuck et al., "Using a fiber stretcher as a fast phase modulator in a continuous wave terahertz spectrometer," *J. Opt. Soc. Am. B* **29**(4), 614–620 (2012).
123. K. Thirunavukkuarasu et al., "Self-normalizing phase measurement in multimode terahertz spectroscopy based on photomixing of three lasers," *Appl. Phys. Lett.* **106**, 031111 (2015).
124. G. Kozlov and A. Volkov, "Coherent source submillimeter wave spectroscopy," in *Millimeter and Submillimeter Wave Spectroscopy of Solids*, Topics in Applied Physics, G. Grüner, Ed., Vol. **74**, pp. 51–109, Springer, Berlin, Heidelberg (1998).
125. G. Mouret et al., "THz media characterization by means of coherent homodyne detection, results and potential applications," *Appl. Phys. B* **89**(2–3), 395–399 (2007).
126. M. Scheller et al., "Single sampling point detection of frequency modulated terahertz waves," *J. Infrared Millimeter Terahertz Waves* **33**, 36–42 (2012).
127. D. Stanze et al., "Compact CW terahertz spectrometer pumped at 1.5 μm wavelength," *J. Infrared Millimeter Terahertz Waves* **32**(2), 225–232 (2011).
128. K. A. McIntosh et al., "Terahertz photomixing with diode lasers in low-temperature-grown GaAs," *Appl. Phys. Lett.* **67**(26), 3844–3846 (1995).
129. R. Wilk et al., "Terahertz generation with 1064 nm DFB laser diode," *Electron. Lett.* **43**(2), 108–110 (2007).
130. M. Tani et al., "Emission characteristics of photoconductive antennas based on low-temperature- grown GaAs and semi-insulating GaAs," *Appl. Opt.* **36**, 7853–7859 (1997).
131. O. Morikawa, M. Tonouchi, and M. Hangyo, "Generation of terahertz radiation by photomixing with dual- and multiple-mode lasers," *Appl. Phys. Lett.* **76**(12), 1519–1521 (2000).
132. W. F. Passchier et al., "The determination of complex refractive indices with Fourier transform interferometry VI: error analysis of liquid-cell experiments," *Infrared Phys.* **17**(5), 381–391 (1977).
133. H. Lotem, Z. Pan, and M. Dagenais, "Tunable dual-wavelength continuous-wave diode laser operated at 830 nm," *Appl. Opt.* **32**, 5270–5273 (1993).
134. K. S. Lee and C. Shu, "Stable and widely tunable dual-wavelength continuous-wave operation of a semiconductor laser in a novel Fabry Perot grating lens external cavity," *IEEE J. Quantum Electron.* **33**, 2199–2202 (1997).
135. L. C. Wang and L. C. Pan, "Tunable multiterahertz beat signal generation from a two-wavelength laser-diode array," *Opt. Lett.* **20**, 1292–1294 (1995).

Biographies of the authors are not available.